How Orthogonal is LoRa Modulation?

Benkhelifa, F., Bouazizi, Y. & McCann, J.

Original citation & hyperlink:
Benkhelifa, F, Bouazizi, Y & McCann, J 2022, 'How Orthogonal is LoRa Modulation?', IEEE Internet of Things Journal, vol. 9, no. 20, pp. 19928-19944. https://dx.doi.org/10.1109/JIOT.2022.3173060

DOI 10.1109/JIOT.2022.3173060
ESSN 2327-4662

Publisher: IEEE

How Orthogonal is LoRa Modulation?

Fatma Benkhelifa, Member, IEEE, Yathreb Bouazizi, Student Member, IEEE, and Julie A. McCann, Member, IEEE

***Abstract*—In this paper, we provide, for the first time, a comprehensive understanding of LoRa waveform theory in order to quantify its orthogonality. We present LoRa waveform expressions in continuous and discrete time domains, and analyze measures of orthogonality between different LoRa spreading factors (SFs) through cross-correlation functions. The cross-correlation functions are analytically expressed in a general form and they account for diverse configuration parameters (bandwidth, SF, etc.) and different cases of signal displacements (time delay shift, frequency shift, etc.). We quantify their mean and maximum in all time domains. We highlight the impact of the temporal displacement and different bandwidths. The general result is that LoRa modulation is non-orthogonal. Firstly, we observe that for same bandwidths the largest maximum cross-correlation happens for same SF and is equal to 100% due to same symbols; whereas for different bandwidths, the largest maximum cross-correlation is no longer observed at the same SF. Secondly, the maximum cross-correlation is less than 26% between different SFs, is higher for closer SFs and decreases as the difference between SFs increases. After downchirping, the maximum cross-correlation increases and the mean decreases compared to those before downchirping. Moreover, the maximum cross-correlation is insignificantly impacted by the temporal delay which makes it valid to adopt for the performance analysis of both synchronous and asynchronous systems. Finally, we analyze by simulation the bit error probability statistics for different bandwidth ratios and highlight their correlated behaviour with the insights obtained from the maximum cross-correlation expressions.**

***Index Terms*—Chirp modulation, LoRa, orthogonality conditions.**

I. Introduction

Internet of Things is a new paradigm standing for a collection of "things" that are connected to Internet, performing complex monitoring and computational operations using embedded objects (sensors, actuators, processors, etc.), and exchanging data for a plethora of applications [1]. IoT applications cover many aspects of everyday life and can be of personal, commercial, industrial, and governmental use. Examples of IoT applications include environmental monitoring, asset management, smart cities, smart agriculture, healthcare monitoring, etc. [2]. IoT has unveiled an increasing growth with an actual number of 11.3 billion connected IoT in 2020 predicted to reach more than 27 billion IoT connection by 2025 by IoT analytics [3]. The global IoT market is expected to reach $1.567 billion by 2025.

Low power wide area (LPWA) networks have attracted tremendous research and industrial interest as the main drivers of IoT growth. Indeed, 2 billion LPWAN devices are expected to be operating by 2025 [3]. LPWA networks promise low power consumption over long range communication while using low cost devices. Several LPWA technologies are competing to answer the challenging requirements of massive connectivity, broad coverage, and low energy consumption. These technologies range from ultra-narrowband (NB) solutions like Sigfox [4], narrow-band solutions like NB-IoT [5], to wide-band solutions like Long Range (LoRa) [6]. Recently, LoRa has gained attention among both research communities and commercial stakeholders thanks to the trade-off between energy, cost, and data rates, that it offers. LoRa also provides an adaptive rate mechanism to enable the tailoring of configurations to better suit a large array of IoT applications.

LoRa was developed by a French startup company named Cycleo and acquired by Semtech in 2012 [7]. The name of technology LoRa refers to the physical layer stack consisting of its patented modulation scheme [8]. Whereas, LoRa Wide Area Network (LoRaWAN) refers to the network layer protocol maintained by the LoRa Alliance [9]. The technical details, signal processing and the theoretical descriptions of the LoRa modulation scheme, are patented and not publicly disclosed [8]. Few recent papers have tried to provide a comprehensive illustration of LoRa modulation with few basic equations [10]–[12]. Some other current works looked at LoRa without any concrete characterisation of its physical layer configuration [11]–[20].

However, it is important to reveal LoRa's behavioural properties. Theoretical investigation regarding its signal theory is not only useful for the user developer but also for the academic community. For example, such concrete characterisation plays a primordial role of identifying implementation scenarios where LoRa is vulnerable to interference and interception. Additionally, this lack of comprehension has led to a non-universal agreement on the nomenclature of LoRa's modulation scheme. Some researchers tend to use it interchangeably with the chirp spread spectrum (CSS) modulation [10], [12], [21], which is quite different as it is not necessarily band-limited compared to LoRa modulation. Some other researchers refer to it as chirp modulation [15], [22] or frequency modulation [16] or wideband linear frequency modulation [13], and some others assigned to it novel names such as frequency shift chirp modulation (FSCM) [23].

F. Benkhelifa is with the School of Computing, Electronics and Mathematics, Coventry University, Coventry, CV1 5FB, United Kingdom (e-mail: ad8904@coventry.ac.uk).

Y. Bouazizi and J.A. McCann are with the Computing department, Imperial College London, London, SW7 2AZ, Kingdom (e-mail: y.bouazizi18,j.mccann}@imperial.ac.uk).

This work is partially supported by the EPSRC grant "Science of Sensor Systems (S4)" programme (EP/N007565/1), and by the Singapore Ministry of National Development and the National Research Foundation, Prime Minister's Office under the Land and Liveability National Innovation Challenge (L2NIC) Research Programme (L2 NIC Award No. L2NICTDF1-2017-3). Any opinions, findings, and conclusions or recommendations expressed in this material are those of the author(s) and do not reflect the views of the Singapore Ministry of National Development and National Research Foundation, Prime Minister's Office, Singapore.

Manuscript received June, 2021

To the best of the authors' knowledge, there has been no full rigorous signal, theory-based characterisation of LoRa's SF *imperfect orthogonality*. Motivated by this, as well as by the heterogeneity of the spreading factors' co-rejection thresholds used in the literature, we choose to delve further into LoRa modulation properties. The main objective of our work is to provide a better understanding of LoRa orthogonality and investigate whether its non-orthogonality can be described as it is commonly believed or if there is a different/novel way to describe it. The main contributions of this work are summarised as follows:

- We provide a comprehensive description of a LoRa signal theory and we present a general formulation of its waveform expressions in continuous and discrete time domains before and after downchirping. We also provide an illustrative example of transmitted LoRa waveforms in absence/presence of interference and their corresponding Fast Fourier transforms (xFFT) to highlight impact of nonorthogonality for different SFs and bandwidths.
- We derive the analytical expression of the cross-correlation function in continuous/discrete time domains (before and after downchirping) with possible time delays and frequency shift. The provided cross-correlation function expressions are general since they account for diverse cases of displacements (time delay, frequency shift, bandwidth, sampling rate, and initial frequency).
- We analyse the orthogonality conditions between different LoRa spreading factors through the derivation of the maximum and the mean of the cross-correlation functions. We also validate the analytical expressions against numerical evaluations.
- We confirm that LoRa modulation is not perfectly orthogonal and its orthogonality cases depend on the value of the *SF*, bandwidth, time delay, etc.
- For same bandwidths, we observe that: (i) the maximum cross-correlation is 1 for the same SF and is mainly due to the transmission of the same symbols, (ii) the largest maximum cross-correlation between different SFs is 26% before sampling and 20% after sampling, (iii) the maximum cross-correlation is higher for closer SFs and decreases as the difference between SFs increases, (iv) the lower SFs impacts more than the higher SFs, and (v) the maximum cross-correlation after downchirping increases hugely and is given by $\sqrt{\frac{SF_1}{SF_2}}$ for $SF_1 \leq SF_2$ in both continuous and discrete time domains.
- We observe also that the mean of cross-correlation is less than 10% and the largest value is observed by the lowest SFs, and the mean of the cross-correlation in the discrete domain is given by $\frac{1}{\sqrt{SF_1 SF_2}}$ before/after downchirping. For different bandwidths, we observe that the largest maximum cross-correlation is no longer observed for the same SF and that the largest maximum cross-correlation occurs for $SF_2 = SF_1 + \frac{B_2}{B_1}$ for $B_2 > B_1$ and for $SF_2 = \min\left(5, SF_1 - \frac{B_1}{B_2}\right)$ for $B_2 < B_1$.
- To validate the impact of orthogonality coefficients on the performance of packet transmission, we simulate the Bit Error Rate statistics for each spreading factor under both an additive white Gaussian noise (AWGN) and interference from the same or different SF using Matlab simulator. The impact of SFs on their BER statistics validates our work by demonstrating an aligned behaviour with the obtained cross-correlation factors.
- We also run a small experiment composed of two LoRa transmitters and a receiver where we quantify the performance of packet delivery ratio (PDR) and we confirm the alignment of its performance with our derived cross-correlation factors.

II. Related Works

LoRa has captured a lot of research interest to investigate its spectral efficiency [24]–[26], energy efficiency [27]–[29], coverage performance [11], [12], [17]–[20], error probability [13], [14], [30], [31]. Some works were based on real-life experiments [13]–[15], [32]–[34] and on custom-build LoRa simulators [11], [16]; while some others are based on computer simulations [12], [17]–[20], [24]–[29]. Some papers investigate the use of emerging technologies such as energy harvesting [24], [26], [32]–[34], nonorthogonal multiple access techniques [25], [26] in LoRa networks.

However, only few current studies have investigated fundamentals about LoRa signal theory [23], [35]–[37]. These studies were limited to the *perfect orthogonality* case, i.e. interaction between LoRa waveforms happens only within the same spreading factor (SF), and the case with different SFs has yet to be investigated. In what follows, we refer to cases with same SFs having an assumed *perfect orthogonality*, while the use cases with different SFs are referred to as assuming *imperfect orthogonality*. Under the *perfect orthogonality* assumption, LoRa's modulation was investigated either in the continuous time domain (before sampling) [35]–[37] or in the discrete time domain (after sampling) [23], [37] where only synchronous transmissions were studied. In [23], LoRa modulation was described as with a frequency shifting chirp modulation (FSCM) and its uncoded performance was compared to frequency shifting (FSK) modulation with both additive white Gaussian noise (AWGN) and frequency-selective channels. However, the investigation of LoRa's waveform orthogonality was limited to chirps in the discrete time domain for synchronous transmissions, again using the same SFs. In [35], the LoRa waveform was described as chirp spread spectrum (CSS) which is not fully faithful to the modulation described in the LoRa patent. The orthogonality conditions in [35] were derived using the same SF in the continuous time domain only. The authors concluded that the maximum modulation rate achieves the Nyquist signalling rate, but the validity of their results is irrelevant as it cannot be attributable to LoRa. Similarly, [36] tackled the perfect orthogonality scenario for continuous synchronous transmission only and compared the LoRa modulation performance to binary phase shift keying (BPSK) and FSK. Again, in [37], LoRa waveform properties were investigated for both continuous and discrete cases, not only was the perfect case assumed, but they only examined the power spectrum and spectral efficiency and did not give a full picture of LoRa waveform properties in terms

Symbol	Definition
SF	Spreading factor $\in \{5,\ldots,12\}$
k	Symbol $\in \{0,\ldots,2^{SF}-1\}$
B	Bandwidth $\in \{125kHz, 250kHz, 500kHz\}$
T	$1/B$
$T_s = T2^{SF}$	Transmission time
f_{min}	Initial frequency
t_0	Starting time
t_k	Shrink point of symbol k
$\phi_k(\cdot)$	Instantaneous phase of symbol k
$f_k(\cdot)$	Instantaneous frequency of symbol k
τ	Time delay
f_d	Differential frequency shift
T_d	Sampling time
$s_k^{\mathcal{C}}(\cdot)$	Continuous waveform of symbol k
$s_{d,k}^{\mathcal{C}}(\cdot)$	Continuous waveform of symbol k after downchirping
$s_k^{\mathcal{D}}(\cdot)$	Discrete waveform of symbol k
$s_{d,k}^{\mathcal{D}}(\cdot)$	Discrete waveform of symbol k after downchirping

TABLE I: List of Notations

of other performance metrics such as bit error rate, or packet delivery ratio. [23], [35], [37] examined the orthogonality conditions when same SF is used and different symbols are transmitted and concluded that LoRa is orthogonal in the discrete time domain while nonorthogonal in the continuous time domain.

The validity of the aforementioned works is questionable given their assumptions of *perfect orthogonality*, especially since recent publications are now describing that LoRa's modulation as "imperfect", "quasi", and "pseudo". Yet no research has quantified *"how orthogonal is LoRa's modulation?"*. Several works have used the assumption of nonorthogonality in their research, but without running a rigorous characterisation [11], [17], [19], [24], [25], [38]–[40]. A first initiative in investigating LoRa's *imperfect orthogonality* was conducted in [11] where the authors derived the co-rejection thresholds between two SFs. The co-rejection thresholds were derived through Matlab simulations and experimental analysis of the bit error rate (BER) of a desired user transmitting with a certain SF in the presence of only one interfering user, using either a different or the same SF. This approach neglects the impact of noise, although there is an interdependence between the signal to interference ratio (SIR) threshold and the LoRa receiver sensitivity, as emphasised in [31]. Further, the obtained co-rejection thresholds become inapplicable when more than one interfering user is present, especially in a massive connectivity scenario.

Considering the limitations of related works, this paper proposes to provide a theoretical-foundation of LoRa signal theory and characterise its orthogonality in function of different physical layer parameters (SF, Bandwidth, initial frequency, etc.) as well as in function of different cases of displacements (time delay, frequency shift, etc.).

III. LoRa Technology: Overview

LoRa operates in the licence-free frequency spectrum. Initially, LoRa was developed to use the sub-GHz band. Its exact range varies from one region to the other. For instance, LoRa uses the EU industrial, scientific, and medical (ISM) frequency bands like 433 MHz and $863-870$ MHz in Europe, $915-928$ MHz in Australia, $902-928$ MHz in North America and Southeast Asia, $915-928$ MHz in Asia, etc. [7]. Within this, there are eight physical configurations: six with spreading factors from 7 to 12 with a bandwidth of 125 kHz each, additionally one with SF 7 on 250 kHz, and another providing Gaussian frequency-shift keying (GFSK) allowing a 50 kbps data rate. Recently, LoRa frequency ranges have been extended and new chips operating in the 2.4 GHz band have been introduced in the market [41]. While LoRa's physical layer stack is private, LoRa's network layer stack, LoRaWAN, is open to public and is maintained by the LoRa Alliance. For the medium access control (MAC), LoRa end devices access the channel using a pure ALOHA-like protocol to transmit their packets.

LoRa's physical layer consists of a *chirp spread spectrum (CSS)*-based modulation scheme also defined in some works as a frequency shifting chirp modulation [23]. An important parameter of this modulation is the spreading factor which defines the number of bits to be encoded in a symbol (i.e. a chirp). The spreading factor influences the data rate, hence, the time a transmitted packet spends on air. In the literature, there are discussions indicating that these spreading factors are pseudo or quasi orthogonal. These declarations were frequently interpreted as follows: (i) user transmissions assigned to different spreading factors do not interfere, and (ii) those within the same spreading factor are able to overcome interference when their signal strength is sufficiently higher than the interferer. In order to check the validity of these technologies and whether there is a novel way to describe its nonorthgonality, this work aims to characterize and provide a better understanding of LoRa orthogonality that was never provided in the literature. Table I states the list of notations used throughout the paper.

IV. LoRa Modulation: Waveforms and Properties

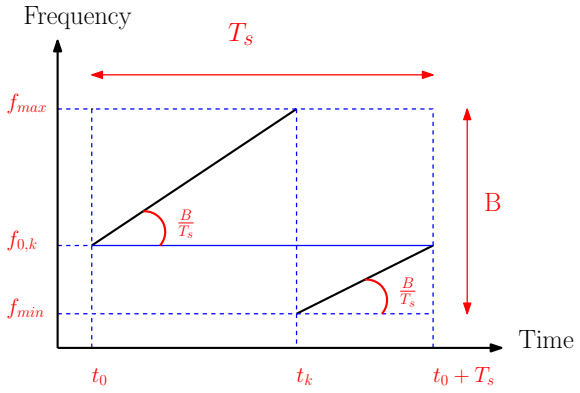

Fig. 1: LoRa Modulation

The principle of the LoRa modulation is known to be based on varying frequency over time (see Fig. 1). The frequency variation starts at an initial time t_0 from an initial frequency f_k (related to the transmitted symbol k) and whenever it reaches the maximum frequency f_{max}, it starts again from the minimum frequency f_{min} and varies again the frequency until the

transmission time ends. The difference between f_{max} and f_{min} is equal to the bandwidth $B \in \{125 \text{ kHz}, 250 \text{ kHz}, 500 \text{ kHz}\}$.

For LoRa, SF is an integer number belonging to the space $\{5,\ldots,12\}$. The slope of the frequency variation is defined by which SF is used and is equal to $\frac{B}{T_s}$, where T_s is the transmission time and is equal to $T_s = 2^{SF}T$ and $T = \frac{1}{B}$. For each SF, we have 2^{SF} number of possible symbols, i.e. $k \in \{0,1,2,\ldots,2^{SF}-1\}$. The symbol k is a binary number of length equal to the spreading factor SF. The symbol k defines the initial frequency f_k expressed as $f_k = f_{min} + k\frac{B}{2^{SF}}$. The symbol k defines also the shrink point t_k in the time domain $[t_0, t_0+T_s]$ as

$$t_k = T\left(2^{SF} - k\right). \tag{1}$$

It should be noted that the frequency at which starts the variation f_k is the same as the frequency at which ends the variation.

A. Continuous-Time Domain

The instantaneous frequency variation standing for each symbol k during T_s is given as

$$f_k(t) = \begin{cases} f_{min} + \frac{B}{2^{SF}}\left(\frac{t-t_0}{T} + k\right), & \text{if } 0 \le t-t_0 \le t_k, \\ f_{min} + \frac{B}{2^{SF}}\left(\frac{t-t_0}{T} + k - 2^{SF}\right), & \text{if } t_k \le t-t_0 \le T_s, \end{cases} \tag{2}$$

$$= f_{min} + \frac{B}{2^{SF}} \mod \left(\frac{t-t_0}{T} + k, 2^{SF}\right), \tag{3}$$

where $\mod(x,y)$ is the modulo operator that gives the rest of the integer division between x and y. Given that $\phi_k(t_0) = 0$, the instantaneous phase can be written as

$$\phi_k(t) = \phi_k(t_0) + \int_{t_0}^{t} f_k(\tau)d\tau \tag{4}$$

$$= \begin{cases} \left(f_{min} + \frac{B}{2^{SF}}\left(\frac{t-t_0}{2T} + k\right)\right)(t-t_0), \\ \qquad\qquad \text{if } 0 \le t-t_0 \le t_k, \\ \left(f_{min} + \frac{B}{2^{SF}}\left(\frac{t-t_0}{2T} + k - 2^{SF}\right)\right)(t-t_0), \\ \qquad\qquad \text{if } t_k \le t-t_0 \le T_s. \end{cases}$$

Property 1. *The instantaneous phase of the LoRa modulated continuous waveform has a memoryless property only if $f_{min} \propto \frac{1}{2^{SF}T}$, i.e.*

$$\phi_k(t_0+T_s) = \left(f_{min} + \frac{B}{2^{SF}}\left(\frac{t_0+T_s-t_0}{2T} + k - 2^{SF}\right)\right) \times (t_0+T_s-t_0) = f_{min}2^{SF}T \mod 2\pi. \tag{5}$$

Subsequently, the continuous waveform $s_k^{\mathcal{C}}(t)$ corresponding to the k'th symbol transmitted during T_s is given by

$$s_k^{\mathcal{C}}(t) = \frac{1}{\sqrt{T_s}} e^{j2\pi\phi_k(t)} \tag{6}$$

$$= \begin{cases} \frac{1}{\sqrt{T_s}} e^{2j\pi\left(f_{min} + \frac{B}{2^{SF}}\left(\frac{t-t_0}{2T} + k\right)\right)(t-t_0)}, & \text{if } 0 \le t-t_0 \le t_k, \\ \frac{1}{\sqrt{T_s}} e^{2j\pi\left(f_{min} + \frac{B}{2^{SF}}\left(\frac{t-t_0}{2T} + k - 2^{SF}\right)\right)(t-t_0)}, & \text{if } t_k \le t-t_0 \le T_s. \end{cases}$$

If we multiply $s_k^{\mathcal{C}}(t)$ by the down chirp using the same SF, the dechirped continuous waveform is given by

$$s_{d,k}^{\mathcal{C}}(t) = \begin{cases} e^{2j\pi\left(2f_{min} + B + \frac{B}{2^{SF}}k\right)(t-t_0)}, & \text{if } 0 \le t-t_0 \le t_k, \\ e^{2j\pi\left(2f_{min} + \frac{B}{2^{SF}}k\right)(t-t_0)}, & \text{if } t_k \le t-t_0 \le T_s. \end{cases} \tag{7}$$

B. Discrete-Time Domain

We sample the transmitted waveform $\tilde{s}_k(t)$ corresponding to the symbol k with a sampling rate $1/T_d$. Ideally, if $T_d = T$, we obtain 2^{SF} samples at time instants $t = nT$ where $n \in \{0,1,\ldots,2^{SF}-1\}$. Otherwise, we get $\frac{T_s}{T_d}$ number of samples. The n'th sample of the continuous transmitted waveform $s_k^{\mathcal{C}}(t)$ corresponding to the k'th symbol can be written as

$$s_k^{\mathcal{D}}(nT_d) = \begin{cases} \frac{1}{\sqrt{2^{SF}}} e^{2j\pi\left(f_{min} + \frac{B}{2^{SF}}\left(\frac{nT_d-t_0}{2T} + k\right)\right)(nT_d-t_0)}, \\ \qquad\qquad \text{if } 0 \le n\frac{T_d}{T} - \frac{t_0}{T} \le 2^{SF}-k-1, \\ \frac{1}{\sqrt{2^{SF}}} e^{2j\pi\left(f_{min} + \frac{B}{2^{SF}}\left(\frac{nT_d-t_0}{2T} + k - 2^{SF}\right)\right)(nT_d-t_0)}, \\ \qquad\qquad \text{if } 2^{SF}-k \le n\frac{T_d}{T} - \frac{t_0}{T} \le 2^{SF}-1. \end{cases} \tag{8}$$

Remark 1. *If $T_d = T$ and t_0 is a multiple of T, i.e. $t_0/T = m_0$, then,*

$$s_k^{\mathcal{D}}(nT) = \frac{1}{\sqrt{2^{SF}}} e^{2j\pi f_{min}(n-m_0)T} e^{2j\pi\left(\frac{n-m_0}{2} + k\right)\frac{n-m_0}{2^{SF}}}. \tag{9}$$

Also, if f_{min} is a multiple of B, then $s_k^{\mathcal{D}}(nT)$ further simplifies to $s_k^{\mathcal{D}}(nT) = \frac{1}{\sqrt{2^{SF}}} e^{2j\pi\left(\frac{n-m_0}{2} + k\right)\frac{n-m_0}{2^{SF}}}$.

If we multiply $s_k^{\mathcal{D}}(nT_d)$ by the down chirp using the same SF, the n'th sample of the dechirped transmitted waveform corresponding to the k'th symbol is given by

$$s_{d,k}^{\mathcal{D}}(nT_d) = \begin{cases} \frac{1}{\sqrt{2^{SF}}} e^{2j\pi\left(2f_{min} + B + \frac{B}{2^{SF}}k\right)(nT_d-t_0)}, \\ \qquad\qquad \text{if } 0 \le n\frac{T_d}{T} - \frac{t_0}{T} \le 2^{SF}-k-1, \\ \frac{1}{\sqrt{2^{SF}}} e^{2j\pi\left(2f_{min} + \frac{B}{2^{SF}}k\right)(nT_d-t_0)}, \\ \qquad\qquad \text{if } 2^{SF}-k \le n\frac{T_d}{T} - \frac{t_0}{T} \le 2^{SF}-1, \end{cases} \tag{10}$$

Remark 2. *If t_0 is a multiple of T, i.e. $t_0/T = m_0$, then,*

$$s_{d,k}^{\mathcal{D}}(nT) = \frac{1}{\sqrt{2^{SF}}} e^{4j\pi f_{min}(n-m_0)T} e^{2j\pi k\frac{n-m_0}{2^{SF}}}. \tag{11}$$

Also, if f_{min} is a multiple of B and $t_0/T = m_0$, then

$$s_{d,k}^{\mathcal{D}}(nT) = \frac{1}{\sqrt{2^{SF}}} e^{2j\pi k\frac{n-m_0}{2^{SF}}}. \tag{12}$$

C. Illustrative Example of LoRa Nonorthogonality

In this part, we present an illustrative example using LoRa Matlab simulator (more details in Section VII) to highlight LoRa nonorthogonality and support the objective of this work. Fig. 2 shows the spectrogram of a sequence of chirps corresponding to the symbols $\{0, 50, 75, 125\}$ and modulated using SF_1 =7. We can see how the chirp varies with the symbol and how the initial frequency varies as the symbol increases. We can see also that the frequency whenever reaches the maximum frequency, resets back to the minimum frequency.

In Fig. 3, we have plotted the FFT amplitude of a LoRa chirp modulated using $SF_1 = 7$ under different interference scenarios. In Fig. 3a, the chirp is sent through an AWGN channel (no interference), while in the remaining subplots we have a simultaneous transmitted interfering chirp modulated using SF_2 over bandwidth B_2 with a SIR value 0 dB. We can see how the peak in the amplitude spectrum is impacted by the interfering SF_2 as well as by the bandwidth B_2. For the interfering scenarios in Fig. 3b and 3d, the interfering signal is weak and the decoding of the desired signal at the receiver is still successful as the peak of FFT amplitude spectrum is similar to the non interference case in Fig. 3a. For the interfering scenarios in Figs. 3c and 3e, the interfering signal is strong enough to diminish the decoding of the desired signal at the receiver. As such, the peak of FFT amplitude spectrum does not correspond always to the same-SF interfering signal.

We believe that identifying impacting interference scenarios is directly correlated with the values of SF and bandwidth of the interfering signal and how different they are from those of the desired signal, which is the objective of this work.

V. Cross Correlation Functions

In this section, we propose to derive the cross-correlation between two LoRa waveforms transmitting two symbols k_1 using SF_1 and k_2 using SF_2 over bandwidths B_1 and B_2, respectively, in the continuous and discrete time domains. The corresponding symbol transmission times are $T_{s,1}$ and $T_{s,2}$ and let $T_j = 1/B_j$, with $j = 1,2$. The starting frequencies of symbols k_1 and k_2 are f_1 and f_2, respectively. Let us assume $SF_1 < SF_2$ and $SF_2 = SF_1 + s$, with $s \in \{1,\dots,7\}$. We aim to examine the orthogonality conditions as well as some other properties.

A. Continuous-Time Domain

First, we study the continuous time domain. The cross-correlation function between the two continuous waveforms is defined as

$$\mathcal{R}^{\mathcal{C}}_{k_1,k_2}(\tau, f_d) = \int_{t_0+\tau}^{t_0+T_{s,1}} s^{\mathcal{C}}_{k_1}(t)\left(s^{\mathcal{C}}_{k_2}(t-\tau)\right)^* dt. \quad (13)$$

where τ is the time delay (TD) and f_d is the frequency differential shift (DFS) between the starting frequencies, i.e. $f_d = f_2 - f_1$.

Theorem 1. *The cross-correlation between two continuous transmitted waveforms is expressed by (14), where*

$$\mathcal{K}_{a_{12}}\left(b_{k_1,k_2}, t_1, t_2\right) \quad (15)$$
$$= \begin{cases} \frac{e^{2j\pi c_{k_2}} e^{-j\pi \frac{b^2_{k_1,k_2}}{a_{12}}}}{\sqrt{T_{s,1}T_{s,2}}} \left[erf\left(\sqrt{\frac{\pi a_{12}}{j}}\left(t_0 + t_2 + \frac{b_{k_1,k_2}}{a_{12}}\right)\right) \right. \\ \left. - erf\left(\sqrt{\frac{\pi a_{12}}{j}}\left(t_0 + t_1 + \frac{b_{k_1,k_2}}{a_{12}}\right)\right)\right], \quad \text{if } a_{12} \neq 0, \\ \frac{e^{2j\pi c_{k_2}} e^{j\pi b_{k_1,k_2}(2t_0+t_1+t_2)} sinc\left(\pi b_{k_1,k_2}(t_2-t_1)\right)(t_2-t_1)}{\sqrt{T_{s,1}T_{s,2}}}, \text{ if } a_{12} = 0, \end{cases}$$

with $\mu_j = \frac{B_j}{2^{SF_j}}$ *for* $j = 1,2$, $a_{12} = \frac{\mu_1}{T_1} - \frac{\mu_2}{T_2}$, $b_{k_1,k_2} = f_1 + \mu_1 k_1 - f_2 - \mu_2 k_2 + \frac{\mu_2 \tau}{T_2}$, $c_{k_2} = \left(f_2 + \mu_2 k_2 - \frac{\mu_2 \tau}{2T_2}\right)\tau$, $m_{k_1,k_2}(\tau) = \min\left(t_{k_1}, \tau + t_{k_2}\right)$, $M_{k_1,k_2}(\tau) = \max\left(t_{k_1}, \tau + t_{k_2}\right)$, *and* $B_c = B_1 u\left(t_{k_2} + \tau - t_{k_1}\right) - B_2 u\left(t_{k_1} - t_{k_2} - \tau\right)$, *$u(\cdot)$ is the step function, and $\mathbb{1}(\cdot)$ is the indicator function.*

Proof. The proof is in Appendix B. □

Corollary 1. *If we denote by* $\mathcal{L}_a(t_1,t_2) = \frac{e^{2j\pi a t_2} - e^{2j\pi a t_1}}{a}$, *the cross-correlation between two continuous transmitted waveforms reduces to (16) if the condition $a_{12} = 0$ is satisfied, i.e.* $\frac{\mu_1}{T_1} = \frac{\mu_2}{T_2}$.

Proof. The proof is an immediate result of Theorem 1. □

Corollary 2. *The cross-correlation between two continuous dechirped transmitted waveforms* $\mathcal{R}^{\mathcal{C}}_{d,k_1,k_2}(\tau, f_d)$ *is also given by (16) but after substituting* $\tilde{c}_{k_2} = (2f_2 + B_2 + \mu_2 k_2)\tau$ *instead of* c_{k_2} *and* $\tilde{b}_{k_1,k_2} = \mu_1 k_1 - \mu_2 k_2 + 2f_1 - 2f_2 + B_1 - B_2$ *instead of* b_{k_1,k_2}.

Proof. The proof follows the same procedure in Appendix B and using Appendix C. □

Corollary 3. *The maximum cross-correlation between two continuous synchronized transmitted waveforms over the same SF with no time delay and no differential frequency shift is equal to*

$$|\mathcal{R}^{\mathcal{C}}_{k_1,k_2}(0,0)| = \frac{2^{SF}}{\pi} \frac{|\sin\left(\pi \frac{(k_1-k_2)^2}{2^{SF}}\right)|}{|k_1-k_2|\left(2^{SF} - |k_1-k_2|\right)} \leq \frac{1}{\pi\left(\sqrt{\frac{2^{SF}}{2}} - \frac{1}{2}\right)}, \quad (17)$$

which happens at $|k_1 - k_2| = \left\lfloor \sqrt{\frac{2^{SF}}{2}} \right\rfloor$ *and* $|k_1 - k_2| = 2^{SF} - \left\lfloor \sqrt{\frac{2^{SF}}{2}} \right\rfloor$, *is upper bounded by* 0.0909 *for* $SF = 5,\dots,12$, *and vanishes as SF goes to infinity.*

Proof. The proof is in Appendix D. □

1) Special Cases

Few special cases can be derived from the general expression in (14).

- Same SF with no TD and no DFS: If $SF_1 = SF_2 = SF$, $B_1 = B_2 = B$, $\tau = 0$, and $f_d = 0$, the cross correlation function becomes

$$\mathcal{R}^{\mathcal{C}}_{k_1,k_2}(0,0) = \frac{e^{\frac{2j\pi}{2^{SF}}(k_1-k_2)\left(\frac{t_0}{T} - k_1\right)}}{2j\pi} \left[\frac{e^{2j\pi\kappa_0 \frac{t_0}{T}}}{2^{SF} - |k_1-k_2|} + \frac{1}{|k_1-k_2|} \right] \times \left(1 - e^{\frac{2j\pi}{2^{SF}}(k_1-k_2)^2}\right), \quad (18)$$

  with $\kappa_0 = \frac{k_2-k_1}{|k_2-k_1|}$.
- Same SF with no TD and with DFS: If $SF_1 = SF_2 = SF$, $B_1 = B_2 = B$, $\tau = 0$, and $f_d \neq 0$, the cross correlation function becomes

$$\mathcal{R}^{\mathcal{C}}_{k_1,k_2}(0,f_d) = \frac{e^{\frac{2j\pi}{2^{SF}}\left(k_1 - k_2 - \frac{f_d 2^{SF}}{B}\right)\left(\frac{t_0}{T} + 2^{SF}\right)}}{2j\pi} \left[\frac{1 - e^{2j\pi \frac{f_d 2^{SF}}{B}}}{k_1 - k_2 - \frac{f_d 2^{SF}}{B}} \right.$$

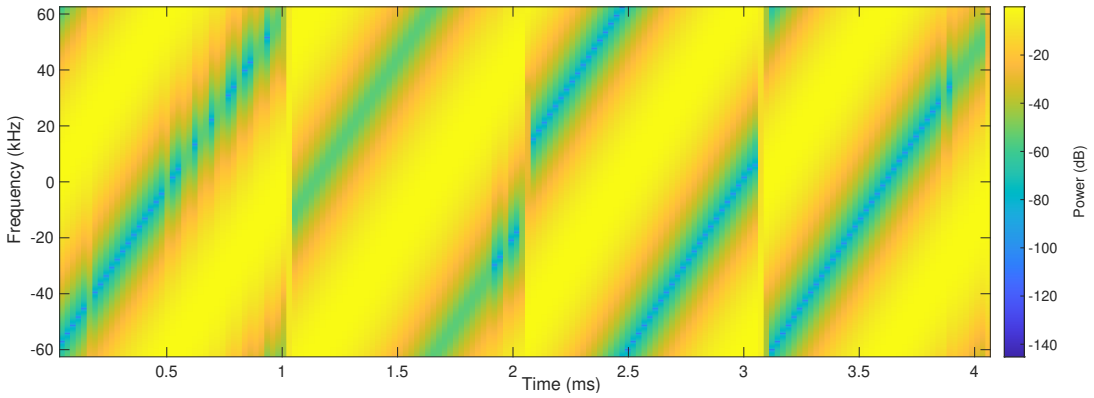

Fig. 2: Spectrogram of a LoRa symbols sequence $\{0,50,75,125\}$ modulated with $SF_1 = 7$ and $B_1 = 125$ KHz.

$$+\left(e^{-\frac{2j\pi}{2^{SF}}\left(k_1-k_2-\frac{f_d 2^{SF}}{B}\right)k_2}-e^{-\frac{2j\pi}{2^{SF}}\left(k_1-k_2-\frac{f_d 2^{SF}}{B}\right)k_1}\right)$$
$$\times\left[\frac{\kappa_0}{k_1-k_2-\frac{f_d 2^{SF}}{B}}-\frac{e^{2j\kappa_0\pi\frac{t_0}{T}}}{2^{SF}+\kappa_0\left(k_1-k_2-\frac{f_d 2^{SF}}{B}\right)}\right]\Bigg]. \quad (19)$$

- Different SFs with no TD and no DFS: If $B_2 = 2^s B_1$ (i.e. $T_2 = 2^{-s}T_1$) and $SF_2 = SF_1 + 2s$ such that $a_{12} = 0$, the cross correlation function becomes as given in (20), with $A = k_1 - 2^{-s}k_2 + \frac{\tau}{T_1} - \frac{f_d}{\mu_1}$.

After examining these special cases, we were able to deduce some orthogonality cases in Table II.

B. Discrete-Time Domain

Next, we consider the case of discrete transmitted waveforms with different SFs. Let T_d be the sampling time and let $B_1 = 2^{s_1}/T_d$, $B_2 = 2^{s_2}/T_d$, and $SF_2 = SF_1 + s_3$. Let $m_0 = \frac{t_0}{T_d}$, and $m_1 = \frac{\tau}{T_d}$.

Theorem 2. *The cross correlation between two discrete transmitted waveforms with different SFs is*

$$\mathcal{R}^{\mathcal{D}}_{k_1,k_2}(\tau, f_d) = \quad (21)$$
$$\begin{cases} \frac{e^{2j\pi c_{k_2}} e^{-j\pi a_{12}\left(\frac{b_{k_1,k_2}}{a_{12}}\right)^2}}{\sqrt{2^{SF_1}2^{SF_2}}} \sum_{n'=m_1}^{2^{SF_1-s_1}-1} e^{j\pi a_{12}\left(n'T_d+\frac{b_{k_1,k_2}}{a_{12}}\right)^2}, & \text{if } a_{12}\neq 0, \\ \frac{e^{2j\pi c_{k_2}} e^{2j\pi b_{k_1,k_2}T_d m_1} e^{j\pi\left(2^{SF_1-s_1}-m_1-1\right)b_{k_1,k_2}T_d}}{\sqrt{2^{SF_1}2^{SF_2}}} cosec\left(\pi b_{k_1,k_2}T_d\right) & \\ \times \sin\left(\pi\left(2^{SF_1-s_1}-m_1\right)b_{k_1,k_2}T_d\right), & \text{if } a_{12}=0 \& b_{k_1,k_2}\neq 0, \\ \frac{e^{2j\pi c_{k_2}}}{\sqrt{2^{SF_1}2^{SF_2}}}\frac{T_{s,1}-\tau}{T_d}, & \text{if } a_{12}=0 \& b_{k_1,k_2}=0, \end{cases}$$

Proof. The proof is in Appendix E. □

Theorem 3. *The cross correlation between two dechirped discrete transmitted waveforms with different SFs is*

$$\mathcal{R}^{\mathcal{D}}_{d,k_1,k_2}(\tau, f_d) \quad (22)$$
$$= \begin{cases} \frac{e^{2j\pi\tilde{c}_{k_2}} e^{2j\pi\tilde{b}_{k_1,k_2}\tau}}{\sqrt{2^{SF_1}2^{SF_2}}} e^{j\pi\left(2^{SF_1-s_1}-m_1-1\right)\tilde{b}_{k_1,k_2}T_d} & \\ \times \sin\left(\pi\left(2^{SF_1-s_1}-m_1\right)\tilde{b}_{k_1,k_2}T_d\right) & \\ \times cosec\left(\pi\tilde{b}_{k_1,k_2}T_d\right), & \text{if } \tilde{b}_{k_1,k_2}\neq 0, \\ \frac{e^{2j\pi\tilde{c}_{k_2}}}{\sqrt{2^{SF_1}2^{SF_2}}}\frac{T_{s,1}-\tau}{T_d}, & \text{if } \tilde{b}_{k_1,k_2}=0, \end{cases}$$

Proof. The proof follows similar steps as in Appendix E. □

Corollary 4. *If both symbols are i.i.d., the mean of the cross correlation between two discrete transmitted waveforms with different SFs is*

$$E_{k_1,k_2}\left[\mathcal{R}^{\mathcal{D}}_{k_1,k_2}\right] = \begin{cases} \frac{1}{\sqrt{2^{SF_1}2^{SF_2}}}, & \text{if } \tau = 0, \\ 0, & \text{if } \tau \neq 0. \end{cases} \quad (23)$$

The same result applies to the mean of the cross correlation between two dechirped discrete synchronized transmitted waveforms with different SFs.

VI. Cross-Correlation Factors

In this section, we aim to characterize the cross-correlation factors of LoRa modulation, in terms of mean and maximum of cross-correlation functions over all possible symbols, as well its cumulative distribution function. We aim also to study the impact of time delay and different bandwidths on the maximum cross-correlation functions. In all the plots, we have compared the analytical and numerical evaluation of cross-correlation function and we have verified their agreement.

A. Maximum, Mean and CDF of Cross-Correlation Functions

In Fig. 4, we plotted the maximum cross-correlation functions in the continuous and discrete time domain before and after down-chirping with $\tau = 0$ and $f_d = 0$. These plots were validated analytically and numerically. The numerical values which led to this figure are also provided in Tables III-V. We observed a couple of properties:

- In both time domains (continuous and discrete), the maximum cross-correlation between the same SFs is more significant than the maximum cross-correlation between

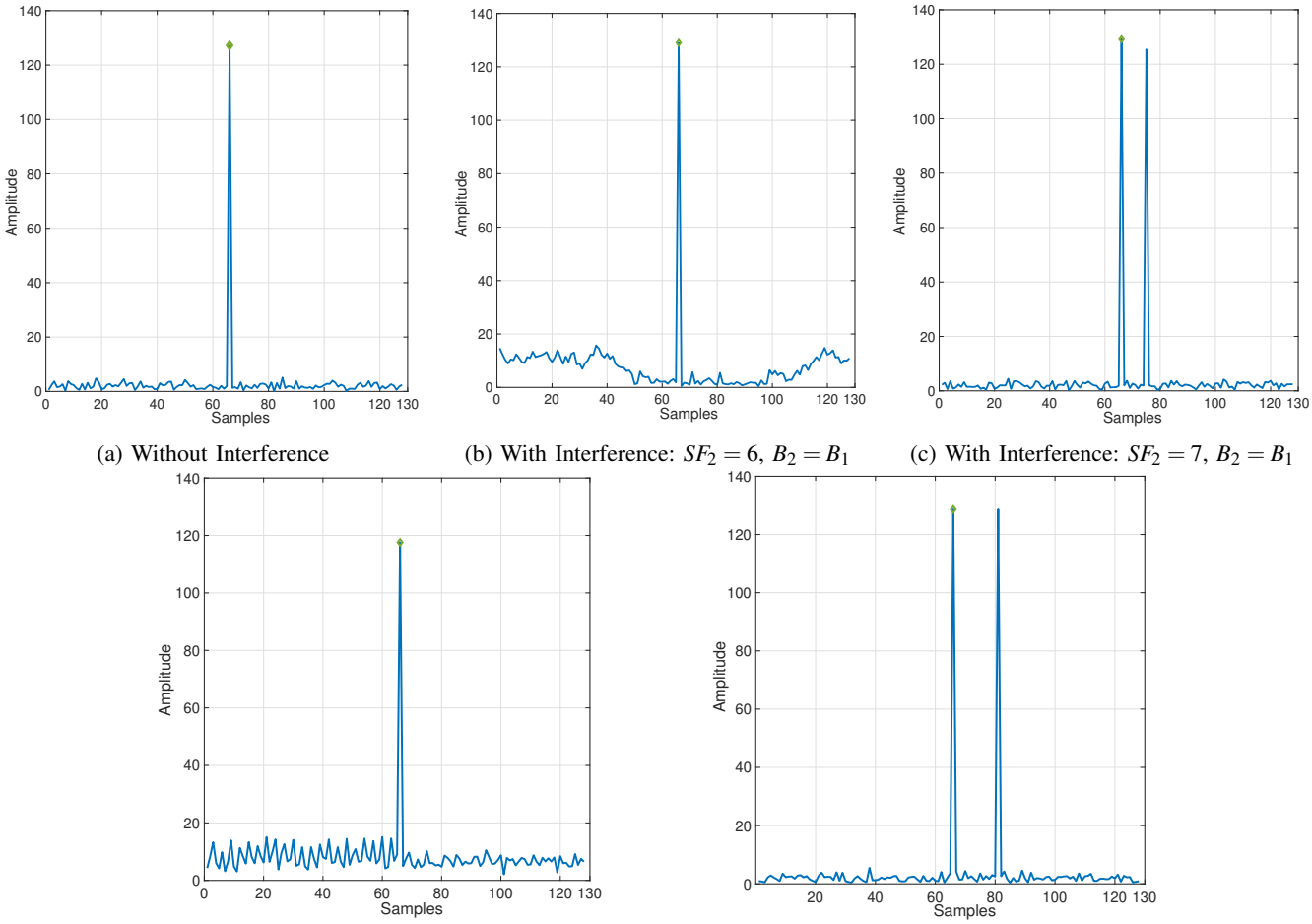

(a) Without Interference (b) With Interference: $SF_2 = 6$, $B_2 = B_1$ (c) With Interference: $SF_2 = 7$, $B_2 = B_1$

(d) With Interference: $SF_2 = 7, B_2 = 2 \times B_1$ (e) With Interference: $SF_2 = 9, B_2 = 2 \times B_1$

Fig. 3: FFT amplitude spectrum of received signal transmitted using $SF_1 = 7$ under (a) only AWGN channel ($SNR = 0$ dB) and (b)-(e) different interference scenarios ($SIR = 0$ dB)

$$\mathcal{R}^{C}_{k_1,k_2}(\tau, f_d) = \begin{cases} \mathcal{K}_{a12}\left(b_{k_1,k_2} - B_1, \tau, T_{s,1}\right), & \text{if } t_{k_1} \le \tau < T_{s,1} \le \tau + t_{k_2}, \\ \mathcal{K}_{a12}\left(b_{k_1,k_2} - B_1, \tau, \tau + t_{k_2}\right) + e^{-2j\pi B_2 \tau}\mathcal{K}_{a12}\left(b_{k_1,k_2} - B_1 + B_2, \tau + t_{k_2}, T_{s,1}\right), & \text{if } t_{k_1} \le \tau < \tau + t_{k_2} < T_{s,1}, \\ \mathcal{K}_{a12}\left(b_{k_1,k_2}, \tau, t_{k_1}\right) + \mathcal{K}_{a12}\left(b_{k_1,k_2} - B_1, t_{k_1}, T_{s,1}\right), & \text{if } \tau < t_{k_1} < T_{s,1} \le \tau + t_{k_2}, \\ \mathcal{K}_{a12}\left(b_{k_1,k_2}, \tau, m_{k_1,k_2}(\tau)\right) + e^{-2j\pi B_2 \tau u\left(t_{k_1} - \tau - t_{k_2}\right)}\mathcal{K}_{a12}\left(b_{k_1,k_2} - B_c, m_{k_1,k_2}(\tau), M_{k_1,k_2}(\tau)\right)\mathbb{1}\left(t_{k_1} - \tau \ne t_{k_2}\right) & \\ + e^{-2j\pi B_2 \tau}\mathcal{K}_{a12}\left(b_{k_1,k_2} - B_1 + B_2, M_{k_1,k_2}(\tau), T_{s,1}\right), & \text{if } \tau < t_{k_1} \& \tau + t_{k_2} < T_{s,1}. \end{cases} \tag{14}$$

$$\mathcal{R}^{C}_{k_1,k_2}(\tau, f_d) = \begin{cases} \frac{e^{2j\pi\left(c_{k_2} + b_{k_1,k_2} t_0 - \frac{t_0}{T_1}\right)}}{2j\pi\sqrt{T_{s,1}T_{s,2}}}\mathcal{L}_{b_{k_1,k_2} - B_1}\left(\tau, T_{s,1}\right), & \text{if } t_{k_1} \le \tau < T_{s,1} \le \tau + t_{k_2}, \\ \frac{e^{2j\pi\left(c_{k_2} + b_{k_1,k_2} t_0 - \frac{t_0}{T_1}\right)}}{2j\pi\sqrt{T_{s,1}T_{s,2}}}\left[\mathcal{L}_{b_{k_1,k_2} - B_1}\left(\tau, \tau + t_{k_2}\right) + e^{2j\pi B_2 (t_0 - \tau)}\mathcal{L}_{b_{k_1,k_2} - B_1 + B_2}\left(\tau + t_{k_2}, T_{s,1}\right)\right], & \text{if } t_{k_1} \le \tau < \tau + t_{k_2} < T_{s,1}, \\ \frac{e^{2j\pi\left(c_{k_2} + b_{k_1,k_2} t_0\right)}}{2j\pi\sqrt{T_{s,1}T_{s,2}}}\left[\mathcal{L}_{b_{k_1,k_2}}\left(\tau, t_{k_1}\right) + e^{-2j\pi\frac{t_0}{T_1}}\mathcal{L}_{b_{k_1,k_2} - B_1}\left(t_{k_1}, T_{s,1}\right)\right], & \text{if } \tau < t_{k_1} < T_{s,1} \le \tau + t_{k_2}, \\ \frac{e^{2j\pi\left(c_{k_2} + b_{k_1,k_2} t_0\right)}}{2j\pi\sqrt{T_{s,1}T_{s,2}}}\Big[\mathcal{L}_{b_{k_1,k_2}}\left(\tau, m_{k_1,k_2}(\tau)\right) + e^{-2j\pi\left(B_2 \tau u\left(t_{k_1} - \tau - t_{k_2}\right) + B_c t_0\right)}\mathcal{L}_{b_{k_1,k_2} - B_c}\left(m_{k_1,k_2}(\tau), M_{k_1,k_2}(\tau)\right)\mathbb{1}\left(t_{k_1} - \tau \ne t_{k_2}\right) & \\ + e^{2j\pi\left(-B_2\tau + (-B_1 + B_2)t_0\right)}\mathcal{L}_{b_{k_1,k_2} - B_1 + B_2}\left(M_{k_1,k_2}(\tau), T_{s,1}\right)\Big], & \text{if } \tau < t_{k_1} \& \tau + t_{k_2} < T_{s,1}. \end{cases} \tag{16}$$

$$\mathcal{R}^{\mathcal{C}}_{k_1,k_2}(\tau, f_d) \tag{20}$$

$$= \begin{cases} \frac{e^{2j\pi c_{k_2}} e^{\frac{2j\pi A}{2^{SF_1}} \frac{t_0}{T_1}}}{2j\pi\sqrt{2^s}} \left[\mathcal{L}_A\left(\frac{\tau}{2^{SF_1}T_1}, \frac{2^s\left(2^{SF_1}-\frac{k_2}{2^{2s}}\right)+\frac{\tau}{T_1}}{2^{SF_1}}\right) + e^{2j\pi\frac{-2^s\tau+2^s t_0}{T_1}} \mathcal{L}_{A+2^s2^{SF_1}}\left(\frac{2^s\left(2^{SF_1}-\frac{k_2}{2^{2s}}\right)+\frac{\tau}{T_1}}{2^{SF_1}}, \frac{2^{SF_1}-k_1}{2^{SF_1}}\right) \right. \\ \left. + e^{2j\pi\frac{-2^s\tau+\left(-1+2^s\right)t_0}{T_1}} \mathcal{L}_{A-2^{SF_1}+2^s2^{SF_1}}\left(\frac{2^{SF_1}-k_1}{2^{SF_1}}, 1\right) \right], & \text{if } \tau < \tau + t_{k_2} \le t_{k_1} < T_{s,1}, \\ \frac{e^{2j\pi c_{k_2}} e^{\frac{2j\pi A}{2^{SF_1}} \frac{t_0}{T_1}}}{2j\pi\sqrt{2^s}} \left[\mathcal{L}_A\left(\frac{\tau}{2^{SF_1}T_1}, \frac{2^{SF_1}-k_1}{2^{SF_1}}\right) + e^{-\frac{2j\pi t_0}{T_1}} \mathcal{L}_{A-2^{SF_1}}\left(\frac{2^{SF_1}-k_1}{2^{SF_1}}, \frac{2^s\left(2^{SF_1}-\frac{k_2}{2^{2s}}\right)+\frac{\tau}{T_1}}{2^{SF_1}}\right) \right. \\ \left. + e^{2j\pi\frac{-2^s\tau+\left(-1+2^s\right)t_0}{T_1}} \mathcal{L}_{A-2^{SF_1}+2^s2^{SF_1}}\left(\frac{2^s\left(2^{SF_1}-\frac{k_2}{2^{2s}}\right)+\frac{\tau}{T_1}}{2^{SF_1}}, 1\right) \right], & \text{if } \tau < t_{k_1} < \tau + t_{k_2} < T_{s,1}, \\ \frac{e^{2j\pi c_{k_2}} e^{\frac{2j\pi A}{2^{SF_1}} \frac{t_0}{T_1}}}{2j\pi\sqrt{2^s}} \left[\mathcal{L}_A\left(\frac{\tau}{2^{SF_1}T_1}, \frac{2^{SF_1}-k_1}{2^{SF_1}}\right) + e^{-2j\pi\frac{t_0}{T_1}} \mathcal{L}_{A-2^{SF_1}}\left(\frac{2^{SF_1}-k_1}{2^{SF_1}}, 1\right) \right], & \text{if } \tau < t_{k_1} < T_{s,1} \le \tau + t_{k_2}, \\ \frac{e^{2j\pi c_{k_2}} e^{\frac{2j\pi A}{2^{SF_1}} \frac{t_0}{T_1}}}{2j\pi\sqrt{2^s}} e^{-\frac{2j\pi t_0}{T_1}} \left[\mathcal{L}_{A-2^{SF_1}}\left(\frac{\tau}{2^{SF_1}T_1}, \frac{2^s\left(2^{SF_1}-\frac{k_2}{2^{2s}}\right)+\frac{\tau}{T_1}}{2^{SF_1}}\right) + e^{2j\pi\frac{-2^s\tau+2^s t_0}{T_1}} \mathcal{L}_{A-2^{SF_1}+2^s2^{SF_1}}\left(\frac{2^s\left(2^{SF_1}-\frac{k_2}{2^{2s}}\right)+\frac{\tau}{T_1}}{2^{SF_1}}, 1\right) \right], & \text{if } t_{k_1} \le \tau < \tau + t_{k_2} < T_{s,1}, \\ \frac{e^{2j\pi c_{k_2}} e^{\frac{2j\pi A}{2^{SF_1}} \frac{t_0}{T_1}}}{2j\pi\sqrt{2^s}} e^{-\frac{2j\pi t_0}{T_1}} \mathcal{L}_{A-2^{SF_1}}\left(\frac{\tau}{2^{SF_1}T_1}, 1\right), & \text{if } t_{k_1} \le \tau < T_{s,1} \le \tau + t_{k_2}, \end{cases}$$

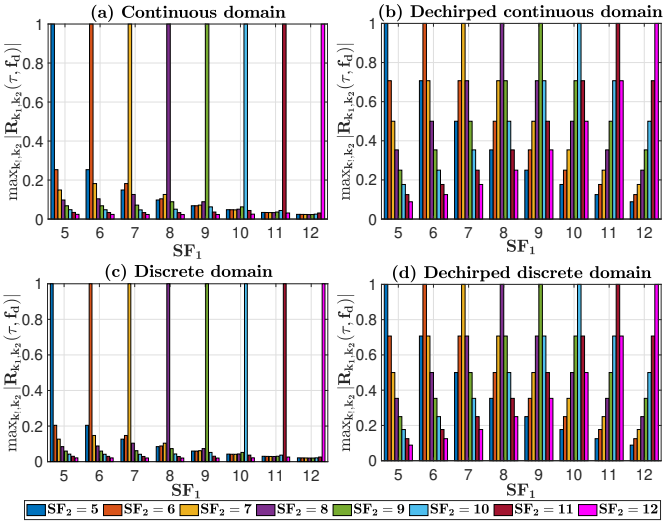

Fig. 4: Maximum of cross-correlation factors between SFs in the continuous/discrete time domains before/after downchirping with $\tau = 0$ and $f_d = 0$.

different SFs. The difference is much larger before down-chirping. This behaviour means that the origin of LoRa non-orthogonality behaviour is due to the same SF and not due to the different SFs. Also, it should be noted that this maximum for the same SF happens when the same symbol is transmitted, i.e. $k_1 = k_2$, otherwise the maximum cross-correlation factor would be almost zero.

- Before down-chirping, lower SFs are more impactful than higher SFs as their maximum cross-correlations are higher. Also, closer SFs impact the maximum cross-correlation more.
- Before down-chirping, the maximum cross-correlation has slightly decreased in the discrete time domain compared to the continuous time domain and this can be explained by the sampling time not being infinitesimally small enough to apply the Riemann integral which approximates the integrals by a sum expression for infinitesimally small steps.
- After down-chirping, the maximum cross-correlation between different SFs has increased compared to those before down-chirping.
- After down-chirping, the maximum cross-correlation between SFs is independent of the time domain, whether continuous or discrete.
- The maximum of the cross-correlation functions after down-chirping is symmetric around the same SF (i.e. $SF_1 = SF_2$) and its exact expression can be mapped to the expression $\sqrt{\frac{SF_1}{SF_2}}$, with $SF_1 \le SF_2$, and it is the same in the continuous and discrete time domain.

In Fig. 5, we have plotted the mean of the cross-correlation functions between SFs in the continuous and discrete time domain, before and after down-chirping, with $\tau = 0$ and $f_d = 0$. These plots were validated analytically and numerically. The numerical values which led to this figure are also provided in Tables VI-VIII. We have also observed several properties:

- In the continuous time domain, the mean cross-correlation is higher than that in the discrete time domain.
- In the continuous time domain, the mean cross-correlation has decreased after down-chirping.
- In the discrete time domain, the mean cross-correlation is the same before and after down-chirping, confirming Corollary 4.

Fig. 6 shows the cumulative distribution function (CDF) of the cross-correlation magnitude in the continuous time domain before/after down-chirping with $SF_1 = 8$. The CDF explains why we see that the mean of cross-correlation of different SFs is higher than that of same SF. Indeed, the same SF has the maximum cross-correlation of 1 for the case of same symbols;

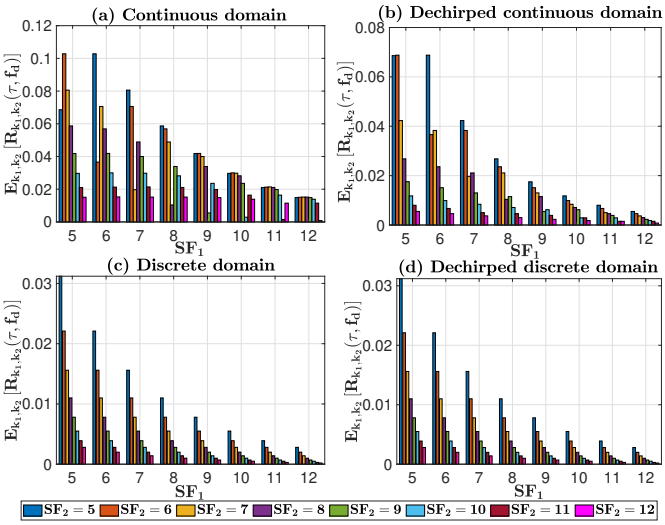

Fig. 5: Mean of cross-correlation factors between SFs in the continuous/discrete time domains before/after downchirping with $\tau = 0$ and $f_d = 0$.

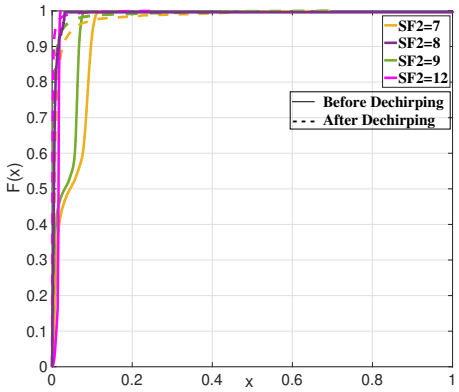

Fig. 6: Cumulative distribution function (CDF) of magnitude of cross-correlation function in the continuous time domain before/after down-chirping with $SF_1 = 8$.

otherwise, the maximum cross-correlation is lower than 0.03 (For $SF = 8$). The CDF justifies also why after dechirping the mean of the cross-correlation function has decreased. We can see how the cross-correlation values span a small interval comparing to the undechipred case. We can see also how the maximum cross-correlation after downchirping is higher than the one before downchirping.

B. Impact of Bandwidth

In Figs. 7 and 8, we have plotted the maximum of the cross-correlation functions for different bandwidth values B_1 and B_2 in the continuous and discrete time domain before and after down-chirping. The sampling rate for the discrete time domain is always equal to $1/B_1$ for both waveforms. We have observed interesting properties:

- The maximum of cross-correlation functions is no longer the largest for the same SF for all time domains.
- The maximum of cross-correlation functions varies only if the ratio $\frac{B_1}{B_2}$ varies. For example, we have the same behaviour for the pairs $B_1 = 125$ kHz and $B_2 = 250$ kHz, and for the pairs $B_1 = 250$ kHz and $B_2 = 500$ kHz.
- Before down-chirping, the maximum cross-correlation behaves similarly for the continuous and discrete time domains. If $B_2 > B_1$, the largest maximum cross-correlation occurs for $SF_2 = SF_1 + \frac{B_2}{B_1}$. For example, for $SF_1 = 5$ and $B_2 = 2 \times B_1$, the maximum cross-correlation is 0.7 which happens at $SF_2 = 7$ while it is less than 0.4 for the other SF_2s.
- If $B_2 < B_1$, the largest maximum cross-correlation happens for $SF_2 = \min\left(5, SF_1 - \frac{B_1}{B_2}\right)$.
- After down-chirping, the largest maximum cross-correlation is obtained for same SF if $B_2 = 2 \times B_1$ and $B_2 = 0.5 \times B_1$.
- The largest maximum cross-correlation occurs for SF_2, not necessarily equal to SF_1, in the discrete time domain after down-chirping. If $B_2 = 2 \times B_1$, the largest maximum is obtained for $SF_2 = 6$. If $B_2 = 4 \times B_1$, it is obtained for $SF_2 = 7$. If $B_2 < B_1$, the largest maximum is obtained for $SF_2 = 5$ independently of SF_1.

C. Impact of Temporal Displacement

In Figs. 9 and 10, we have plotted the maximum of cross-correlation functions versus the time delay for same and different symbols in the continuous and discrete time domains, before and after down-chirping. We have observed a couple of properties that are completely different; before and after performing the down-chirping. The common behavior is that the maximum of the cross-correlation function decreases as the delay increases, except for the case with same SFs and different symbols after down-chirping. Before down-chirping, we have observed in Fig. 9 that:

- For same symbols, the maximum cross-correlation for different SFs is higher than the one for same SFs for both continuous and discrete cases (when τ is not close to zero).
- For same symbols and different SFs, the maximum cross-correlation follows the same values as for the zero time delay scenario, up to a certain value of τ. This observation confirms that the maximum cross-correlation with zero delay can be generalized to the asynchronous case.
- For different symbols, the maximum cross-correlation for the same SFs is higher than half, in both the continuous and discrete time domains, which makes the demodulation process difficult to succeed.
- The maximum cross-correlation for same SFs is higher than that for different SFs in both the continuous and discrete cases (when τ is not close to zero).
- For different symbols and different SFs, the maximum cross-correlation function follows the same value as that for the zero time delay scenario up to a certain value of τ.
- The temporal displacement graphs show that for the same SF in both continuous and discrete time, when τ is perfectly 0 the cross correlation is 0 or near 0 however when τ goes slightly above 0, the cross correlation correlation reaches a pick and this counterintuitively implies

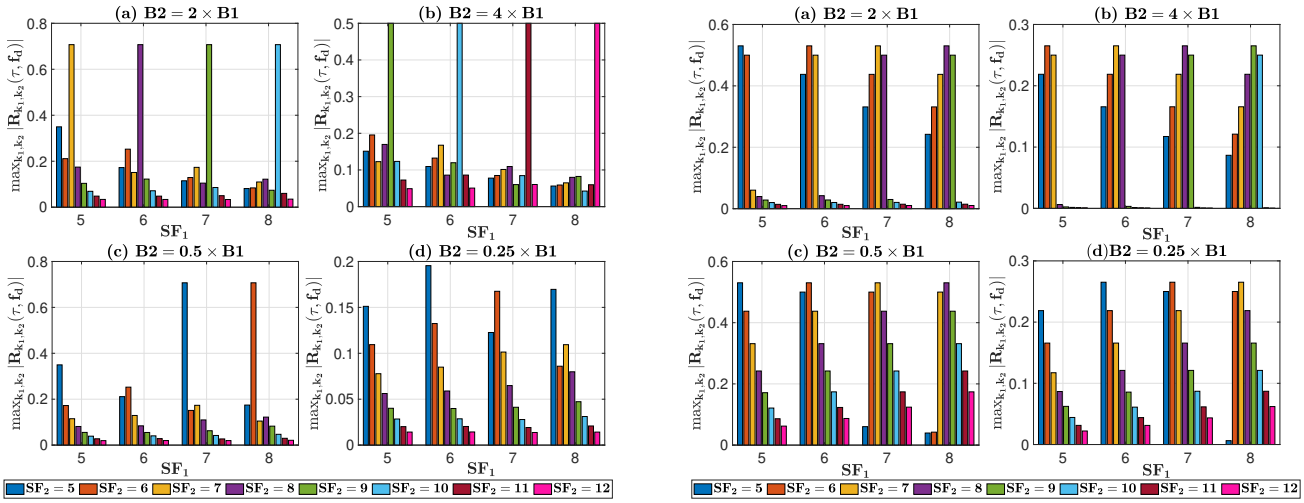

(a) before downchirping (b) after downchirping

Fig. 7: Maximum of cross-correlation factors between SFs in the continuous time domain with $\tau = 0$ and $f_d = 0$ for different B_1 and B_2.

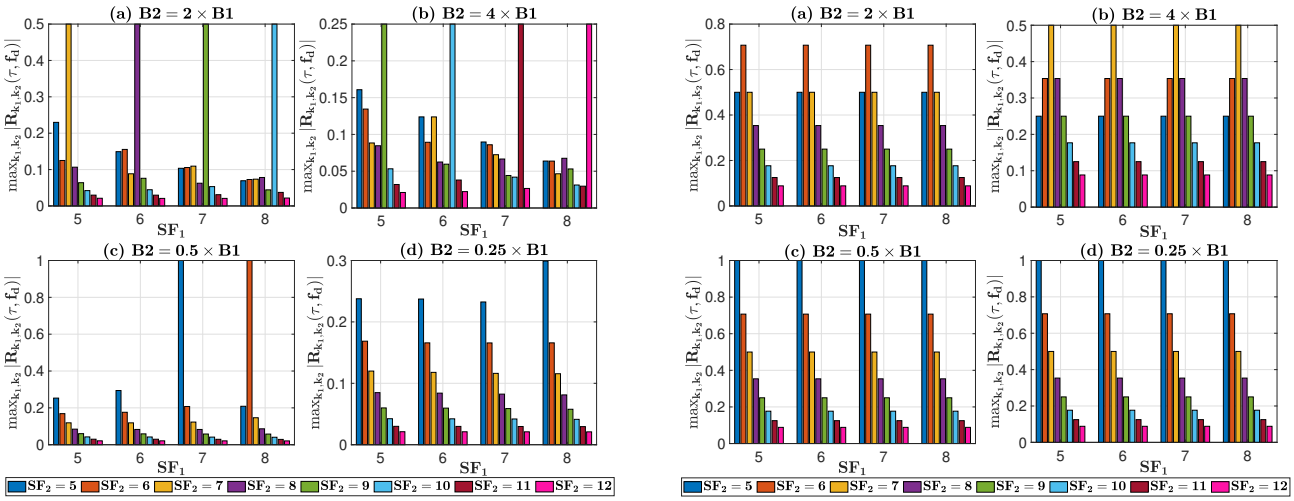

(a) before downchirping (b) after downchirping

Fig. 8: Maximum of cross-correlation factors between SFs in the discrete time domain with $\tau = 0$ and $f_d = 0$ for different B_1 and B_2.

that the probability to decode symbols that are perfectly synchronised could be higher than when they are slightly asynchronous.

After down-chirping, we have observed in Fig. 10 that:

- For same symbols, the maximum cross-correlation is higher for the same SFs than those observed for different SFs in the continuous/discrete cases.
- The maximum of the cross-correlation function achieving higher than half happens only for same SF scenarios and some different SFs (precisely when SF_1 and SF_2 are close) in both the continuous and discrete time domains.
- For different symbols, the maximum cross-correlation being higher than half happens only for different SFs (precisely when SF_1 and SF_2 are close) in both continuous and discrete time domains. For example, the maximum of cross-correlation function between $SF_1 = 6$ and $SF_2 = 7$ are higher than 0.5 for a time delay τ less than $20T_1$. Also, the maximum of cross-correlation function between $SF_1 = 7$ and $SF_2 = 8$ are higher than 0.5 for a time delay τ less than $40T_1$.
- The maximum of cross-correlation function is higher for different SFs than for same SFs in the continuous/discrete cases.
- The maximum of cross-correlation is less than half for the same SFs in both the continuous/discrete case after down-chirping.

VII. Bit Error Rate Analysis

Before LoRa symbols are generated using the LoRa modulation, the message bit sequence goes through a pipeline of operations at the transmitter side and their corresponding inverses at the receiver side. This pipeline includes a Gray

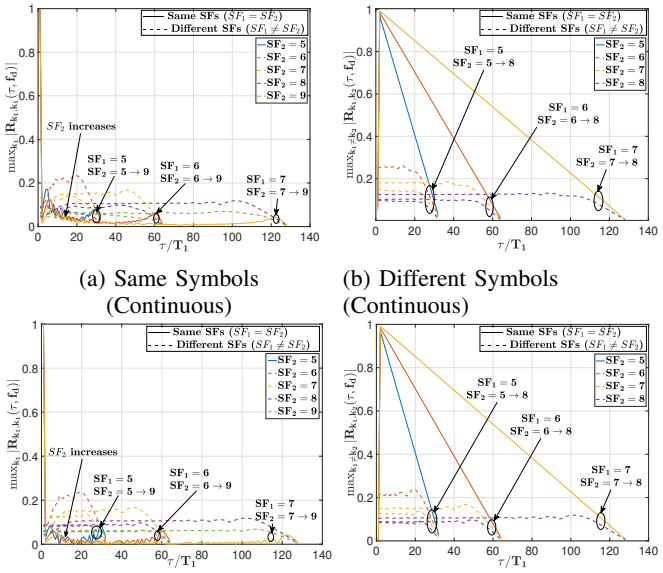

(a) Same Symbols (Continuous) (b) Different Symbols (Continuous)

(c) Same Symbols (Discrete) (d) Different Symbols (Discrete)

Fig. 9: Maximum cross-correlation functions versus time delay τ/T_1 before downchirping.

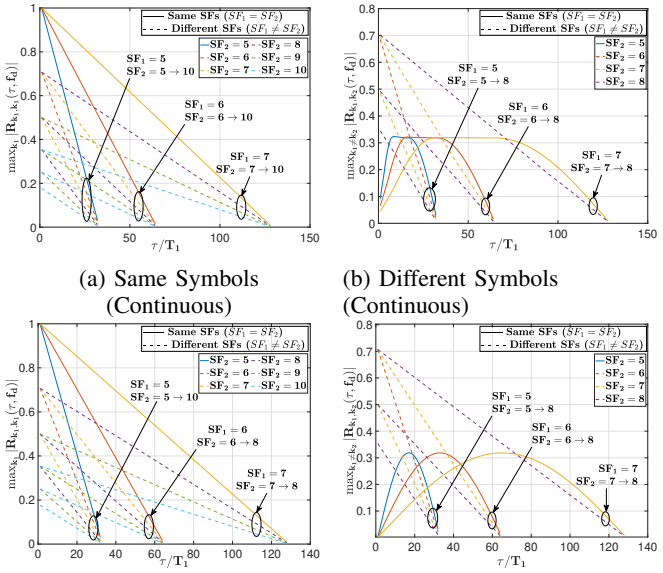

(a) Same Symbols (Continuous) (b) Different Symbols (Continuous)

(c) Same Symbols (Discrete) (d) Different Symbols (Discrete)

Fig. 10: Maximum cross-correlation functions versus time delay τ/T_1 after downchirping.

coding, a Hamming coding operation that ranges from a simple parity check to an extended Hamming code of rate $4/(4+CR)$ based on the chosen coding rate parameter CR$\in \{1,2,3,4\}$ and an interleaving operation that aims to avoid the propagation of adjacent errors through a diagonal interleaver of size $(SF*(CR+4))$ [8]. We built our LoRa's physical layer simulator on Matlab based on the processing pipeline explained in [11], [42]. Fig. 11 shows the BER performance of different spreading factors under an additive white Gaussian channel for the case of a $4/7$ hamming coding scheme. We

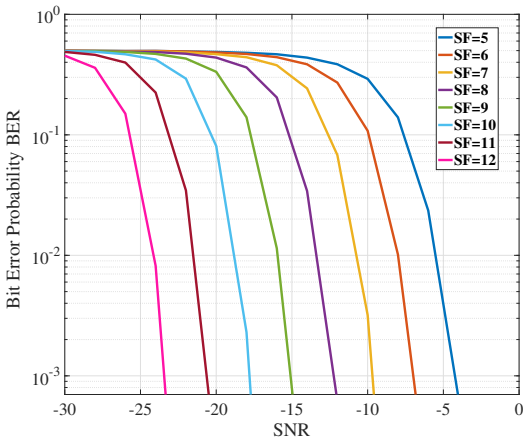

Fig. 11: Coded LoRa BER performance under AWGN for different SFs

choose to conduct the investigation of the orthogonality impact on the BER performance without considering the coding and interleaving operations in order to isolate the impact that these operations may induce on the BER performance.

To account for the inter-relation between noise and the interference highlighted in [31], we evaluate the BER while considering different signal to interference ratios (SIR) and signal to noise ratios (SNR) values. Indeed, we calculate the BER of each SF_1 under both additive white Gaussian noise (AWGN) and a random interfering packet for which we varied its SF_2. For each interfering SF_2, we considered a given SNR value based on the sensitivity range, from Table 1 in [31] of the evaluated SF_1, and we varied the amplitude of the interfering signal by varying its SIR ratio. The desired packet is fixed to N bytes (25 for the following graphs) rounded to a number of blocks. The desired packet information sequence is modulated using SF_1 and then impaired using a second random bit sequence that is modulated using SF_2. The overall received signal $R(nT) = S_0(nT) + S_{int}(nT) + W(nT)$ goes through the demodulation process which is based on a down-chirping operation followed by a Discrete Fourier Transform (DFT) [42]. The decoded symbol is detected by the position of the maximum in the DFT amplitude spectrum of R.

To evaluate the impact of LoRa SFs orthogonality and equate it to the obtained cross-correlation factors detailed in the previous section, we plotted the BER for different combinations of BWs and for different SFs. We found that the behaviour of the BER statistics is aligned with the behaviour of the maximum cross-correlation functions in the discrete time domain. By examining the subplots in Fig. 12, we can see how the dominant SF is not always the same SF as the desired one (i.e. SF_1); it changes based on the BW ratio between the desired and the interfering SF as was shown previously in Fig. 8a. The dominant interfering SF is the one that has the highest cross-correlation factors in Table V.

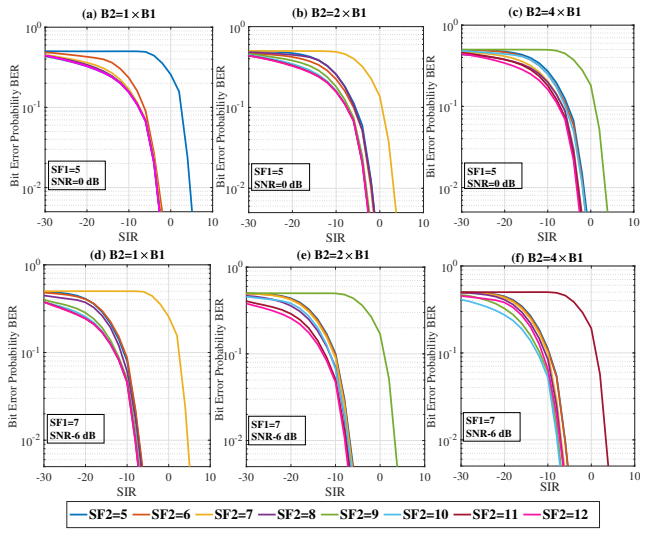

Fig. 12: LoRa BER performance under interference from different SFs before downchirping with $\tau = 0$ and $f_d = 0$ for different B_1 and B_2.

VIII. Experimental Analysis of Packet Delivery Ratio (PDR)

In this section, we run a small experimental setup made up of three LoRa end users (2 transmitters and 1 receiver) in Fig. 13a. Each LoRa end user is represented by Semtech SX1280 2.4GHz transceiver [43]. One transmitter is set to be the desired user and the second transmitter is set to be the interfering user. We set the transmit power of both transmitters to 22 dBm. We varied the SFs and bandwidths of each transmitter and we quantified the packet delivery ratio (PDR) which is defined as the ratio between the correctly received packets over the transmitted packets. In Figs. 13b, 13c, and 14, we have plotted the PDR versus the SF of desired user SF_1 for different values of interferer's SF $SF_2 \in \{5,\dots,12\}$. The SF of desired user SF_1 is between 5 and 12 in Fig. 13b, while it is between 5 and 8 for the others. In Figs. 13b and 13c, we look at the case of same bandwidths at the desired user and interferer. However, in Fig. 14, we look at the case of different bandwidths between the desired user and interferer, i.e. $B_1/B_2 \in \{0.25, 0.5, 2, 4\}$. Firstly, we observe that for the same bandwidths in Figs. 13b and 13c, PDR is performing badly for the same SF and is exactly equal to zero in most cases. This behaviour is highly aligned with the maximum cross-correlation factors for the same SF which we have shown that they are equal to one for the same SF. Secondly, when we have different bandwidths as in Fig. 14, PDR is the worst when the difference between SFs is exactly equal to the ratio between bandwidths when $B_2 > B_1$. This behaviour is explained due to the fact that the maximum cross-correlation factor is the largest for $SF_2 = SF_1 + B_2/B_1$ with $B_2 > B_1$. Also, when $B_2 < B_1$, PDR vanished when $SF_2 = \min\left(5, SF_1 - B_1/B_2\right)$ which is also aligned with the behaviour of our cross-correlation factors.

IX. Summary

In this paper, we provided, for the first time, a general expression of a LoRa waveform transmitting a certain symbol using a specific SF over a certain bandwidth for an initial frequency and a nonzero starting time. We analytically expressed the cross-correlation functions between two LoRa waveforms transmitting two symbols (not necessarily different) using possibly different SFs and bandwidths for a possible time delay and a differential frequency shift. We considered both the continuous and discrete time domains, and before and after downchirping (multiplying with a down chirp at the receiver). Special cases were analyzed for no time delay, no differential frequency shift, or different bandwidths (B_2 multiple of 2 of B_1). Based on the special cases in Section IV-A-1), some orthogonality conditions are summarized in Table II. We have expressed the maximum cross-correlation in the continuous time domain using the same SF, and we have shown that the mean of cross-correlation functions in the discrete time domain is the same before and after downchirping and is given by $\frac{1}{\sqrt{2^{SF_1}2^{SF_2}}}$ for different SFs and zero otherwise. Furthermore, we have numerically evaluated the maximum and mean of cross-correlation functions in continuous/discrete time domains before/after downchirping. For the same bandwidths, we have observed that the largest maximum cross-correlation is obtained by the same SF; whereas, for different bandwidths, the largest maximum cross-correlation is not always obtained by the same SF. For example, if $B_1 > B_2$, the largest maximum cross-correlation happens at $SF_2 = SF_1 + \frac{B_2}{B_1}$. While if $B_2 < B_2$, the largest maximum cross-correlation happens at $SF_2 = \min\left(5, SF_1 - \frac{B_1}{B_2}\right)$.

We have also observed that closer SFs have higher maximum cross-correlation than farther SFs, and the maximum cross correlation after downchirping is symmetric around the same SFs. We deduced that its expression can be fitted to the value $\sqrt{\frac{SF_1}{SF_2}}$ for $SF_1 < SF_2$.

We have examined the non-zero time delays and we have observed that for same symbols, the maximum cross-correlation is higher for different SFs than for same SFs; whereas, for different symbols, the maximum cross-correlation is higher for same SFs than for different SFs. Also, for different SFs, the maximum cross-correlation function has the same value as those with zero time delay for different SFs up to a certain value of time delay τ. The temporal displacement graphs illustrate that the maximum of the cross-correlation functions is insignificantly impacted by the temporal delay which makes it safe to adopt for the performance analysis of both synchronous and asynchronous systems.

To highlight the impact of LoRa nonorthogonality, we simulated the bit error rate of LoRa using a Matlab simulator and we ran a small set of experiment made of three LoRa nodes where we calculated the packet delivery ratio (PDR) metric. We have highlighted that their performance is aligned with the behaviour observed by the maximum cross-correlation factors. To further confirm the orthogonality analysis and properties, we are planning to run extensive experiments to quantify the bit error rate and confirm if its behaviour is exactly aligned with all of our orthogonality conditions.

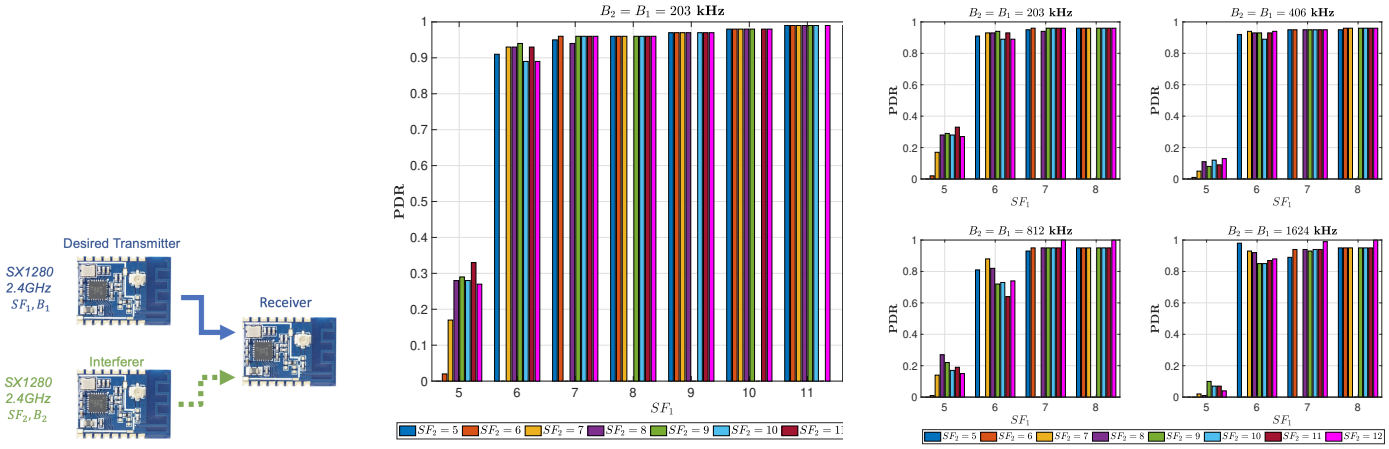

(a) Experimental setup using three LoRa nodes

(b) $B_1 = B_2 = 203$ MHz, $SF_1 \in \{5,\ldots,12\}$ and $SF_2 \in \{5,\ldots,12\}$.

(c) $B_1 = B_2 \in \{203,\ldots,1624\}$ MHz, $SF_1 \in \{5,\ldots,8\}$ and $SF_2 \in \{5,\ldots,12\}$.

Fig. 13: Experimental analysis of packet delivery ratio (PDR) of desired transmitter using same bandwidth and different SFs: (a) experimental setup using Semtech SX1280 2.4GHz transceivers, (b) same bandwidth $B_1 = B_2 = 203$ MHz, and different values of same bandwidths.

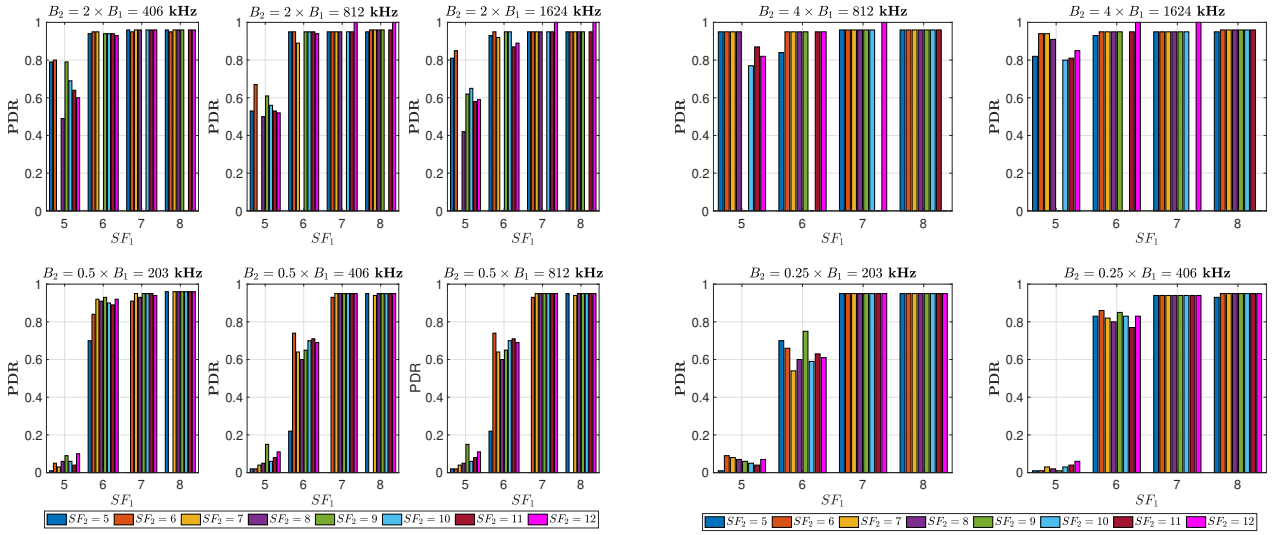

(a) $B_1 = 2B_2$ and $B_1 = 0.5B_2$

(b) $B_1 = 4B_2$ and $B_1 = 0.25B_2$

Fig. 14: Experimental analysis of packet delivery ratio (PDR) of desired transmitter using different bandwidths and different SFs: $SF_1 \in \{5,\ldots,8\}$ and $SF_2 \in \{5,\ldots,12\}$

APPENDIX A

We aim to express the integral

$$I_{k_1,k_2}(\tau,t_1,t_2) \tag{24}$$

$$= \int_{t_1}^{t_2} e^{2j\pi\left(f_1+\mu_1\left(\frac{t}{2T_1}+k_1\right)\right)t} e^{-2j\pi\left(f_2+\mu_2\left(\frac{t-\tau}{2T_2}+k_2\right)\right)(t-\tau)} dt$$

$$= e^{2j\pi\left(f_2+\mu_2 k_2-\frac{\mu_2\tau}{2T_2}\right)\tau} \int_{t_1}^{t_2} e^{2j\pi\left(\mu_1 k_1-\mu_2 k_2+f_1-f_2+\frac{\mu_2\tau}{T_2}\right)t} e^{j\pi\left(\frac{\mu_1}{T_1}-\frac{\mu_2}{T_2}\right)t^2} dt \tag{25}$$

$$= e^{2j\pi c_{k_2}} \int_{t_1}^{t_2} e^{j\pi\left(2b_{k_1,k_2}t+a_{12}t^2\right)} dt \tag{26}$$

$$= \begin{cases} e^{j\pi\left(2c_{k_2}-\frac{b_{k_1,k_2}^2}{a_{12}}\right)} \int_{t_1}^{t_2} e^{j\pi a_{12}\left(t+\frac{b_{k_1,k_2}}{a_{12}}\right)^2} dt, & \text{if } a_{12} \neq 0, \\ e^{2j\pi c_{k_2}} \int_{t_1}^{t_2} e^{2j\pi b_{k_1,k_2}t} dt, & \text{if } a_{12} = 0, \end{cases} \tag{27}$$

$$= \begin{cases} \sqrt{\frac{j}{\pi a_{12}}} e^{j\pi\left(2c_{k_2}-\frac{b_{k_1,k_2}^2}{a_{12}}\right)} \int_{\sqrt{\frac{\pi a_{12}}{j}}\left(t_1+\frac{b_{k_1,k_2}}{a_{12}}\right)}^{\sqrt{\frac{\pi a_{12}}{j}}\left(t_2+\frac{b_{k_1,k_2}}{a_{12}}\right)} e^{-x^2} dx, \\ \qquad \text{if } a_{12} \neq 0, \\ e^{2j\pi c_{k_2}} e^{j\pi b_{k_1,k_2}(t_1+t_2)} \\ \times sinc\left(\pi b_{k_1,k_2}(t_2-t_1)\right)(t_2-t_1), \quad \text{if } a_{12} = 0, \end{cases} \tag{28}$$

TABLE II: Orthogonality Conditions

Time Domain	SFs	Bws	Time Shift	Freq Shift	Orthog. Conditions
Continuous	$SF_1 = SF_2$	$B_1 = B_2$	$\tau = 0$	$f_d = 0$	SF even & $\lvert k_1 - k_2 \rvert \propto \sqrt{2^{SF}}$
				$f_d \neq 0$	SF even & $f_d \propto \frac{B}{2^{SF}}$ &$\lvert k_1 - k_2 - \frac{f_d 2^{SF}}{B} \rvert \propto \sqrt{2^{SF}}$
			$\tau \neq 0$	$f_d = 0$	SF even & $\tau \propto T$ & $\lvert k_1 - k_2 + \frac{\tau}{T} \rvert \propto \sqrt{2^{SF}}$
				$f_d \neq 0$	SF even & $\tau \propto T$ & $f_d \propto \frac{B}{2^{SF}}$ &$\lvert k_1 - k_2 + \frac{\tau}{T} - \frac{f_d 2^{SF}}{B} \rvert \propto \sqrt{2^{SF}}$
Discrete	$SF_1 = SF_2$	$B_1 = B_2$	$\tau = 0$	$f_d = 0$	$k_1 - k_2 \neq 0$
				$f_d \neq 0$	$f_d \propto \frac{B_1}{2^S F_1}$ & $k_1 - k_2 - f_d \frac{2^S F_1}{B_1} \neq 0$
			$\tau \neq 0$	$f_d = 0$	$\left(2^{SF_1} - \tau/T_1\right)\left(k_1 - k_2 + \frac{\tau}{T_1}\right) \propto 2^{SF_1}$
				$f_d \neq 0$	$f_d \propto \frac{B_1}{2^S F_1}$ & $\left(2^{SF_1} - \tau/T_1\right)\left(k_1 - k_2 + \frac{\tau}{T_1} - f_d \frac{2^S F_1}{B_1}\right) \propto 2^{SF_1}$
Dechirped Discrete	$SF_1 = SF_2$	$B_1 = B_2$	$\tau = 0$	$f_d = 0$	$k_1 - k_2 \neq 0$
				$f_d \neq 0$	$f_d \propto \frac{B_1}{2^S F_1}$ & $k_1 - k_2 - 2 f_d \frac{2^S F_1}{B_1} \neq 0$
			$\tau \neq 0$	$f_d = 0$	$\left(2^{SF_1} - \tau/T_1\right)(k_1 - k_2) \propto 2^{SF_1}$
				$f_d \neq 0$	$f_d \propto \frac{B_1}{2^S F_1}$ & $\left(2^{SF_1} - \tau/T_1\right)\left(k_1 - k_2 - 2 f_d \frac{2^S F_1}{B_1}\right) \propto 2^{SF_1}$
	$SF_2 = SF_1 + 2s$	$B_2 = 2^s B_1$	$\tau = 0$	$f_d = 0$	$f_d \propto \frac{B_1}{2^S F_1}$ & $\left(k_1 - \frac{k_2}{2^s} + (1 - 2^s) 2^{SF_1}\right) \neq 0$
				$f_d \neq 0$	$f_d \propto \frac{B_1}{2^S F_1}$ & $\left(k_1 - \frac{k_2}{2^s} - 2 f_d \frac{2^S F_1}{B_1} + (1 - 2^s) 2^{SF_1}\right) \neq 0$
			$\tau \neq 0$	$f_d = 0$	$\left(2^{SF_1} - \tau/T_1\right)\left(k_1 - \frac{k_2}{2^s} + (1 - 2^s) 2^{SF_1}\right) \propto 2^{SF_1}$
				$f_d \neq 0$	$f_d \propto \frac{B_1}{2^S F_1}$ & $\left(2^{SF_1} - \tau/T_1\right)\left(k_1 - \frac{k_2}{2^s} - 2 f_d \frac{2^S F_1}{B_1} + (1 - 2^s) 2^{SF_1}\right) \propto 2^{SF_1}$
	$SF_1 \neq SF_2$	$B_1 \neq B_2$	$\forall \tau$	$\forall f_d$	$f_d \propto \frac{B_1}{2^S F_1}$ & $\left(2^{SF_1} - \tau/T_1\right)\left(k_1 - \frac{B_2 2^{SF_1}}{B_1 2^{SF_2}} k_2 - 2 f_d \frac{2^S F_1}{B_1} + (1 - \frac{B_2}{B_1}) 2^{SF_1}\right) \propto 2^{SF_1}$

$$= \begin{cases} \frac{\sqrt{j}}{2\sqrt{a_{12}}} e^{j\pi\left(2c_{k_2} - \frac{b_{k_1,k_2}^2}{a_{12}}\right)} \left[erf\left(\sqrt{\frac{\pi a_{12}}{j}}\left(t_2 + \frac{b_{k_1,k_2}}{a_{12}}\right)\right) \right. \\ \left. - erf\left(\sqrt{\frac{\pi a_{12}}{j}}\left(t_1 + \frac{b_{k_1,k_2}}{a_{12}}\right)\right)\right], \quad \text{if } a_{12} \neq 0, \\ e^{2j\pi c_{k_2}} e^{j\pi b_{k_1,k_2}(t_1+t_2)} \\ \times sinc\left(\pi b_{k_1,k_2}(t_2 - t_1)\right)(t_2 - t_1), \quad \text{if } a_{12} = 0, \end{cases} \tag{29}$$

with $a_{12} = \frac{\mu_1}{T_1} - \frac{\mu_2}{T_2}$, $b_{k_1,k_2} = \mu_1 k_1 - \mu_2 k_2 + f_1 - f_2 + \frac{\mu_2 \tau}{T_2}$, $c_{k_2} = \left(f_2 + \mu_2 k_2 - \frac{\mu_2 \tau}{2T_2}\right)\tau$.

APPENDIX B
PROOF OF THEOREM 1

The cross-correlation between two continuous transmitted waveforms with different SFs is given by

$$\mathcal{R}^{\mathcal{C}}_{k_1,k_2}(\tau, f_d) = \int_{t_0}^{t_0+T_{s,1}} s^{\mathcal{C}}_{k_1}(t)\left(s^{\mathcal{C}}_{k_2}(t-\tau)\right)^* dt \tag{30}$$

$$= \frac{1}{\sqrt{2^{SF_1} 2^{SF_2}}} \int_{t_0+\tau}^{t_0+T_{s,1}} s^{\mathcal{C}}_{k_1}(t)\left(s^{\mathcal{C}}_{k_2}(t-\tau)\right)^* dt. \tag{31}$$

Let us denote by $\mu_j = \frac{B_j}{2^{SF_j}}$ for $j = 1, 2$, $a_{12} = \frac{\mu_1}{T_1} - \frac{\mu_2}{T_2}$, $b_{k_1,k_2} = f_1 + \mu_1 k_1 - f_2 - \mu_2 k_2 + \frac{\mu_2 \tau}{T_2}$, and $c_{k_2} = \left(f_2 + \mu_2 k_2 - \frac{\mu_2 \tau}{2T_2}\right)\tau$. We have five possible cases based on which we express the cross-correlation function as in (32). Then using Appendix A, we get the results in Theorem 1.

APPENDIX C

We aim to express the integral

$$J_{k_1,k_2}(\tau, t_1, t_2) = \int_{t_1}^{t_2} e^{2j\pi(2f_1 + B_1 + \mu_1 k_1)t} e^{-2j\pi(2f_2 + B_2 + \mu_2 k_2)(t-\tau)} dt \tag{33}$$

$$= e^{2j\pi(2f_2 + B_2 + \mu_2 k_2)\tau} \int_{t_1}^{t_2} e^{2j\pi(\mu_1 k_1 - \mu_2 k_2 + 2f_1 - 2f_2 + B_1 - B_2)t} dt \tag{34}$$

$$= e^{2j\pi\tilde{c}_{k_2}} \int_{t_1}^{t_2} e^{2j\pi\tilde{b}_{k_1,k_2} t} dt \tag{35}$$

$$= \begin{cases} e^{2j\pi\tilde{c}_{k_2}} e^{j\pi\tilde{b}_{k_1,k_2}(t_1+t_2)} \\ \times sinc\left(\pi\tilde{b}_{k_1,k_2}(t_2 - t_1)\right)(t_2 - t_1), & \text{if } \tilde{b}_{k_1,k_2} \neq 0, \\ e^{2j\pi\tilde{c}_{k_2}}(t_2 - t_1), & \text{if } \tilde{b}_{k_1,k_2} = 0, \end{cases} \tag{36}$$

with $\tilde{c}_{k_2} = (2f_2 + B_2 + \mu_2 k_2)\tau$, $\tilde{b}_{k_1,k_2} = \mu_1 k_1 - \mu_2 k_2 + 2f_1 - 2f_2 + B_1 - B_2$.

APPENDIX D
MAXIMUM CROSS-CORRELATION OF CONTINUOUS WAVEFORMS

The argument of the cross-correlation between two continuous synchronized transmitted waveforms over the same SF exists for $0 \leq \lvert k_1 - k_2 \rvert \leq 2^{SF}$ and is given by

$$\lvert \mathcal{R}^{\mathcal{C}}_{k_1,k_2}(0,0) \rvert = \frac{2^{SF}}{\pi} \frac{\lvert \sin\left(\pi \frac{(k_1-k_2)^2}{2^{SF}}\right) \rvert}{\lvert k_1 - k_2 \rvert \left(2^{SF} - \lvert k_1 - k_2 \rvert\right)} \tag{37}$$

$$\mathcal{R}^{\mathcal{C}}_{k_1,k_2}(\tau,f_d)= \tag{32}$$

$$\begin{cases} \frac{1}{\sqrt{T_{s,1}T_{s,2}}}\left[I_{k_1,k_2}\left(\tau,t_0+\tau,t_0+t_{k_1}\right)+I_{k_1-2^{SF_1},k_2}\left(\tau,t_0+t_{k_1},t_0+\tau+t_{k_2}\right)+I_{k_1-2^{SF_1},k_2-2^{SF_2}}\left(\tau,t_0+\tau+t_{k_2},t_0+T_{s,1}\right)\right], & \text{if } \tau<t_{k_1}<\tau+t_{k_2}<T_{s,1},\\ \frac{1}{\sqrt{T_{s,1}T_{s,2}}}\left[I_{k_1,k_2}\left(\tau,t_0+\tau,t_0+\tau+t_{k_2}\right)+I_{k_1,k_2-2^{SF_2}}\left(\tau,t_0+\tau+t_{k_2},t_0+t_{k_1}\right)+I_{k_1-2^{SF_1},k_2-2^{SF_2}}\left(\tau,t_0+t_{k_1},t_0+T_{s,1}\right)\right], & \text{if } \tau<\tau+t_{k_2}<t_{k_1}<T_{s,1},\\ \frac{1}{\sqrt{T_{s,1}T_{s,2}}}\left[I_{k_1,k_2}\left(\tau,t_0+\tau,t_0+t_{k_1}\right)+I_{k_1-2^{SF_1},k_2}\left(\tau,t_0+t_{k_1},t_0+T_{s,1}\right)\right], & \text{if } \tau<t_{k_1}<T_{s,1}<\tau+t_{k_2},\\ \frac{1}{\sqrt{T_{s,1}T_{s,2}}}\left[I_{k_1-2^{SF_1},k_2}\left(\tau,t_0+\tau,t_0+\tau+t_{k_2}\right)+I_{k_1-2^{SF_1},k_2-2^{SF_2}}\left(\tau,t_0+\tau+t_{k_2},t_0+T_{s,1}\right)\right], & \text{if } t_{k_1}<\tau<\tau+t_{k_2}<T_{s,1},\\ \frac{1}{\sqrt{T_{s,1}T_{s,2}}}I_{k_1-2^{SF_1},k_2-2^{SF_2}}\left(\tau,t_0+\tau,t_0+T_{s,1}\right), & \text{if } t_{k_1}<\tau<T_{s,1}<\tau+t_{k_2}. \end{cases}$$

First, $|\mathcal{R}^{\mathcal{C}}_{k_1,k_2}(0,0)|$ is symmetric around $\frac{2^{SF}}{2}$. In addition, the numerator of (37) is an increasing function with respect to $|k_1-k_2|$ whenever we have one of these conditions

$$\sqrt{2^{SF}l}<|k_1-k_2|<\sqrt{2^{SF}\left(l+\frac{1}{2}\right)}, \tag{38}$$

$$\text{for } l=0,1,2,\ldots,2^{SF}-5. \tag{39}$$

Otherwise, it is a decreasing function. The maximums of the numerator of (37) happens at

$$|k_1-k_2|=\left\lfloor\sqrt{2^{SF}\left(l+\frac{1}{2}\right)}\right\rfloor,\ \text{for } l=1,2,3,\ldots,2^{SF}-3. \tag{40}$$

Also, the denominator of (37) is an increasing function for $0\le|k_1-k_2|\le 2^{SF}/2$, and a decreasing function for $2^{SF}/2\le|k_1-k_2|\le 2^{SF}-1$. So, the maximum of $|\mathcal{R}^{\mathcal{C}}_{k_1,k_2}(0,0)|$ should happen at $|k_1-k_2|=\left\lfloor\sqrt{\frac{2^{SF}}{2}}\right\rfloor$ and $|k_1-k_2|=2^{SF}-\left\lfloor\sqrt{\frac{2^{SF}}{2}}\right\rfloor$, and it is equal to

$$\max_{k_1\neq k_2}|\mathcal{R}^{\mathcal{C}}_{k_1,k_2}(0,0)|=\frac{1}{\pi\left(\sqrt{\frac{2^{SF}}{2}}-\frac{1}{2}\right)} \tag{41}$$

$$\underset{SF=5\to 12}{=}\left[9.09,6.17,4.24,2.94,2.05,1.44,1.01,0.71\right]\times 10^{-2}. \tag{42}$$

APPENDIX E
PROOF OF THEOREM 2

Let T_d be the sampling time and let $B_1=2^{s_1}/T_d$, $B_2=2^{s_2}/T_d$, and $SF_2=SF_1+s_3$. Let $m_0=\frac{t_0}{T_d}$, and $m_1=\frac{\tau}{T_d}$. The cross-correlations between two discrete transmitted waveforms is given by

$$\mathcal{R}^{\mathcal{D}}_{k_1,k_2}(\tau,f_d)=\sum_{n=\frac{t_0}{T_d}+\frac{\tau}{T_d}}^{\frac{t_0}{T_d}+\frac{T_{s,1}}{T_d}-1}s^{\mathcal{D}}_{k_1}(nT_d)\left(s^{\mathcal{D}}_{k_2}(nT_d-\tau)\right)^* \tag{43}$$

$$=\frac{e^{2j\pi c_{k_2}}}{\sqrt{2^{SF_1}2^{SF_2}}}\sum_{n=\frac{\tau}{T_d}}^{2^{SF_1-s_1}-1}e^{j\pi 2^{-s_1-SF_1}\left(\left(2^{s_1}-2^{-s_1+2s_2-s_3}\right)n\right)n}\times e^{j\pi 2^{-s_1-SF_1}\left(2\left(A-2^{s_1}1\left(nT_d\ge t_{k_1}\right)+2^{s_2}1\left(nT_d\ge t_{k_2}+\tau\right)\right)\right)n} \tag{44}$$

$$=\begin{cases}\frac{e^{2j\pi c_{k_2}}}{\sqrt{2^{SF_1}2^{SF_2}}}\sum_{n=\frac{\tau}{T_d}}^{\frac{T_{s,1}}{T_d}-1}e^{j\pi a_{12}(nT_d)^2}\times e^{2j\pi\left(b_{k_1,k_2}-B_1 1\left(nT_d\ge t_{k_1}\right)+B_2 1\left(nT_d\ge t_{k_2}+\tau\right)\right)nT_d}, & \text{if } a_{12}\neq 0,\\ \frac{e^{2j\pi c_{k_2}}}{\sqrt{2^{SF_1}2^{SF_2}}}\sum_{n=\frac{\tau}{T_d}}^{\frac{T_{s,1}}{T_d}-1}e^{2j\pi\left(b_{k_1,k_2}-B_1 1\left(nT_d\ge t_{k_1}\right)\right)nT_d}\times e^{2j\pi B_2 1\left(nT_d\ge t_{k_2}+\tau\right)nT_d}, & \text{if } a_{12}=0,\end{cases} \tag{45}$$

$$=\begin{cases}\frac{e^{2j\pi c_{k_2}}}{\sqrt{2^{SF_1}2^{SF_2}}}\sum_{n=\frac{\tau}{T_d}}^{2^{SF_1-s_1}-1}e^{j\pi\left(a_{12}nT_d+2b_{k_1,k_2}\right)nT_d}, & \text{if } a_{12}\neq 0,\\ \frac{e^{2j\pi c_{k_2}}}{\sqrt{2^{SF_1}2^{SF_2}}}\sum_{n=\frac{\tau}{T_d}}^{2^{SF_1-s_1}-1}e^{2j\pi b_{k_1,k_2}nT_d}, & \text{if } a_{12}=0,\end{cases} \tag{46}$$

$$=\begin{cases}\frac{e^{2j\pi c_{k_2}}e^{-j\pi a_{12}\left(\frac{b_{k_1,k_2}}{a_{12}}\right)^2}}{\sqrt{2^{SF_1}2^{SF_2}}}\times\sum_{n'=0}^{2^{SF_1-s_1-m_1-1}}e^{j\pi a_{12}\left(n'T_d+m_1T_d+\frac{b_{k_1,k_2}}{a_{12}}\right)^2}, & \text{if } a_{12}\neq 0,\\ \frac{e^{2j\pi c_{k_2}}e^{2j\pi b_{k_1,k_2}T_d m_1}e^{j\pi\left(2^{SF_1-s_1-m_1-1}\right)b_{k_1,k_2}T_d}}{\sqrt{2^{SF_1}2^{SF_2}}}\times\sin\left(\pi\left(2^{SF_1-s_1}-m_1\right)b_{k_1,k_2}T_d\right)\times cosec\left(\pi b_{k_1,k_2}T_d\right), & \text{if } a_{12}=0\,\&\,b_{k_1,k_2}\neq 0,\\ \frac{e^{2j\pi c_{k_2}}}{\sqrt{2^{SF_1}2^{SF_2}}}\frac{T_{s,1}-\tau}{T_d}, & \text{if } a_{12}=0\,\&\,b_{k_1,k_2}=0,\end{cases} \tag{47}$$

with $m_1=\frac{\tau}{T_d}$, $a_{12}=\frac{\mu_1}{T_1}-\frac{\mu_2}{T_2}=\left(1-2^{2(-s_1+s_2)-s_3}\right)\frac{\mu_1}{T_1}$, $b_{k_1,k_2}=\mu_1\left(k_1-2^{2(-s_1+s_2)-s_3}k_2+2^{2(-s_1+s_2)-s_3}\frac{\tau}{T_1}-\frac{f_d2^{SF_1}}{B_1}\right)$, and $c_{k_2}=\left(f_2+\mu_2k_2-\frac{\tau\mu_2}{2T_2}\right)\tau$.

APPENDIX F
TABLES OF LORA CROSS-CORRELATION FACTORS

In this section, we provide in Tables III-VIII the numerical values of the maximum and mean cross-correlation factors that were validated analytically using our expressed cross-correlation functions and which are the object of the plotted figures 4 and 5 with $\tau=0$, $f_d=0$, and $B_1=B_2$.

TABLE III: Maximum of cross-correlations functons in continuous time domain

	5	6	7	8	9	10	11	12
5	1	0.253	0.149	0.098	0.068	0.048	0.034	0.024
6	0.253	1	0.182	0.104	0.068	0.048	0.034	0.024
7	0.149	0.182	1	0.126	0.072	0.047	0.033	0.024
8	0.098	0.104	0.126	1	0.089	0.051	0.033	0.023
9	0.068	0.068	0.072	0.089	1	0.063	0.036	0.023
10	0.048	0.048	0.047	0.051	0.063	1	0.044	0.025
11	0.034	0.034	0.033	0.033	0.036	0.044	1	0.031
12	0.024	0.024	0.024	0.023	0.023	0.025	0.031	1

TABLE IV: Maximum of cross-correlation functions in continuous & discrete time domains after downchirping

	5	6	7	8	9	10	11	12
5	1	0.707	0.5	0.354	0.25	0.177	0.125	0.088
6	0.707	1	0.707	0.5	0.354	0.25	0.177	0.125
7	0.5	0.707	1	0.707	0.5	0.354	0.25	0.177
8	0.354	0.5	0.707	1	0.707	0.5	0.354	0.25
9	0.25	0.354	0.5	0.707	1	0.707	0.5	0.354
10	0.177	0.25	0.354	0.5	0.707	1	0.707	0.5
11	0.125	0.177	0.25	0.354	0.5	0.707	1	0.707
12	0.088	0.125	0.177	0.25	0.354	0.5	0.707	1

TABLE V: Maximum of cross-correlation functions in discrete time domain

	5	6	7	8	9	10	11	12
5	1	0.204	0.127	0.084	0.059	0.042	0.030	0.021
6	0.204	1	0.147	0.088	0.059	0.042	0.030	0.021
7	0.126	0.147	1	0.104	0.062	0.041	0.029	0.021
8	0.084	0.088	0.104	1	0.073	0.043	0.029	0.020
9	0.059	0.059	0.062	0.073	1	0.052	0.030	0.020
10	0.042	0.042	0.041	0.043	0.052	1	0.037	0.021
11	0.030	0.030	0.029	0.029	0.030	0.037	1	0.026
12	0.021	0.021	0.021	0.020	0.020	0.021	0.026	1

TABLE VI: Mean of crosscorrelation functions in continuous time domain

	5	6	7	8	9	10	11	12
5	0.069	0.103	0.080	0.059	0.042	0.030	0.021	0.015
6	0.103	0.037	0.071	0.057	0.042	0.030	0.022	0.015
7	0.081	0.071	0.020	0.049	0.040	0.030	0.021	0.015
8	0.059	0.057	0.049	0.010	0.034	0.028	0.021	0.015
9	0.042	0.042	0.040	0.034	0.006	0.024	0.020	0.015
10	0.030	0.030	0.030	0.028	0.024	0.003	0.016	0.014
11	0.021	0.021	0.021	0.021	0.020	0.016	0.002	0.012
12	0.015	0.015	0.015	0.015	0.015	0.014	0.012	0.001

TABLE VII: Mean of crosscorrelation functions in continuous time domain after downchirping

	5	6	7	8	9	10	11	12
5	0.067	0.069	0.042	0.027	0.018	0.012	0.008	0.006
6	0.069	0.037	0.038	0.024	0.015	0.010	0.007	0.005
7	0.042	0.038	0.020	0.021	0.013	0.008	0.005	0.004
8	0.027	0.024	0.021	0.010	0.012	0.007	0.005	0.003
9	0.018	0.015	0.013	0.012	0.006	0.006	0.004	0.002
10	0.012	0.010	0.008	0.007	0.006	0.003	0.003	0.002
11	0.008	0.007	0.005	0.005	0.004	0.003	0.002	0.002
12	0.006	0.005	0.004	0.003	0.002	0.002	0.002	0.001

TABLE VIII: Mean of crosscorrelation functions in discrete time domain before & after downchirping

	5	6	7	8	9	10	11	12
5	0.031	0.022	0.016	0.011	0.008	0.006	0.004	0.003
6	0.022	0.016	0.011	0.008	0.006	0.004	0.003	0.002
7	0.016	0.011	0.008	0.006	0.004	0.003	0.002	0.001
8	0.011	0.008	0.006	0.004	0.003	0.002	0.001	0.001
9	0.008	0.006	0.004	0.003	0.002	0.001	0.001	0.001
10	0.006	0.004	0.003	0.002	0.001	0.001	0.001	0.001
11	0.004	0.003	0.002	0.001	0.001	0.001	0.001	0.0003
12	0.003	0.002	0.001	0.001	0.001	0.001	0.0003	0.0002

ACKNOWLEDGMENT

The authors would like to thank the anonymous reviewers for their feedback. The authors would like also to thank Dr. Takoua Jendoubi from University College London (UCL), London, UK, for the constructive discussions that initiated the idea of this work. The authors would like also to thank Mr. Laksh Bhatia from Imperial College London, London, UK, for the experimental data that he provided to support this work

REFERENCES

[1] [Online]. Available: https://iot-analytics.com/Internet-of-things-definition/
[2] L. Atzori, A. Iera, and G. Morabito, "The internet of things: A survey," *Computer Networks*, vol. 54, no. 15, pp. 2787–2805, 2010. [Online]. Available: https://www.sciencedirect.com/science/article/pii/S1389128610001568
[3] [Online]. Available: https://iot-analytics.com/number-connected-iot-devices/
[4] Sigfox. [Online]. Available: https://www.sigfox.com
[5] Y. P. E. Wang, X. Lin, A. Adhikary, A. Grovlen, Y. Sui, Y. Blankenship, J. Bergman, and H. S. Razaghi, "A primer on 3GPP narrowband Internet of Things," *IEEE Communications Magazine*, vol. 55, no. 3, pp. 117–123, March 2017.
[6] S. Corporation. LoRa modulation basics - AN1200.22, revision 2. [Online]. Available: https://www.semtech.com/uploads/documents/an1200.22.pdf
[7] Semtech. [Online]. Available: https://www.semtech.com
[8] O. Bernard, A. Seller, and N. Sornin, "Low power long range transmitter," 2014.
[9] [Online]. Available: https://lora-alliance.org/
[10] C. Goursaud and J.-M. Gorce, "Dedicated networks for IoT : PHY / MAC state of the art and challenges," *EAI endorsed transactions on Internet of Things*, Oct. 2015. [Online]. Available: https://hal.archives-ouvertes.fr/hal-01231221
[11] D. Croce, M. Gucciardo, S. Mangione, G. Santaromita, and I. Tinnirello, "Impact of LoRa imperfect orthogonality: Analysis of link-level performance," *IEEE Communications Letters*, vol. 22, no. 4, pp. 796–799, April 2018.
[12] M. C. Bor, U. Roedig, T. Voigt, and J. M. Alonso, "Do LoRa low-power wide-area networks scale?" in *Proceedings of the 19th ACM International Conference on Modeling, Analysis and Simulation of Wireless and Mobile Systems (MSWiM '2016)*, Nov. 2016, pp. 59–67.
[13] D. Yim, J. Chung, Y. Cho, H. Song, D. Jin, S. Kim, S. Ko, A. Smith, and A. Riegsecker, "An experimental LoRa performance evaluation in tree farm," in *IEEE Sensors Applications Symposium (SAS'2018)*, 2018, pp. 1–6.
[14] N. Jovalekic, V. Drndarevic, E. Pietrosemoli, I. Darby, and M. Zennaro, "Experimental study of LoRa transmission over seawater," *Sensors*, vol. 18, no. 9, 2018. [Online]. Available: https://www.mdpi.com/1424-8220/18/9/2853
[15] L. Gregora, L. Vojtech, and M. Neruda, "Indoor signal propagation of LoRa technology," in *17th International Conference on Mechatronics - Mechatronika (ME'2016)*, 2016, pp. 1–4.
[16] T. Voigt, M. Bor, U. Roedig, and J. Alonso, "Mitigating inter-network interference in LoRa networks," in *Proceedings of the 2017 International Conference on Embedded Wireless Systems and Networks*, ser. EWSN '17. USA: Junction Publishing, 2017, p. 323–328.

[17] Y. Bouazizi, F. Benkhelifa, and J. McCann, "Spatiotemporal modelling of multi-gateway LoRa networks with imperfect SF orthogonality," in *GLOBECOM 2020 - 2020 IEEE Global Communications Conference*, 2020, pp. 1–7.
[18] Z. Qin, Y. Liu, G. Y. Li, and J. A. McCann, "Modelling and analysis of low-power wide-area networks," in *IEEE International Conference on Communications (ICC'2017)*, May 2017, pp. 1–7.
[19] A. Waret, M. Kaneko, A. Guitton, and N. El Rachkidy, "LoRa throughput analysis with imperfect spreading factor orthogonality," *IEEE Wireless Communications Letters*, vol. 8, no. 2, pp. 408–411, April 2019.
[20] L. Beltramelli, A. Mahmood, M. Gidlund, P. Österberg, and U. Jennehag, "Interference modelling in a multi-cell LoRa system," in *14th International Conference on Wireless and Mobile Computing, Networking and Communications (WiMob'2018)*, October 2018, pp. 1–8.
[21] A. Carlsson, I. Kuzminykh, R. Franksson, and A. Liljegren, "Measuring a LoRa network: Performance, possibilities and limitations," in *Internet of Things, Smart Spaces, and Next Generation Networks and Systems*, O. Galinina, S. Andreev, S. Balandin, and Y. Koucheryavy, Eds. Cham: Springer International Publishing, 2018, pp. 116–128.
[22] C. E. Cook, "Linear FM signal formats for beacon and communication systems," *IEEE Transactions on Aerospace and Electronic Systems*, vol. AES-10, no. 4, pp. 471–478, 1974.
[23] L. Vangelista, "Frequency Shift Chirp Modulation: The LoRa Modulation," *IEEE Signal Processing Letters*, vol. 24, no. 12, pp. 1818–1821, 2017.
[24] F. Benkhelifa, Z. Qin, and J. McCann, "Minimum throughput maximization in LoRa networks powered by ambient energy harvesting," in *IEEE International Conference on Communications (ICC'2019)*, Shanghai, China, May 2019, pp. 1–7.
[25] K. Li, F. Benkhelifa, and J. McCann, "Resource allocation for non-orthogonal multiple access (NOMA) enabled LPWA networks," in *IEEE Global Communications Conference (GLOBECOM'2019)*, 2019, pp. 1–6.
[26] F. Benkhelifa and J. McCann, "Resource allocation for NOMA-based LPWA networks powered by energy harvesting," in *IEEE Wireless Communications and Networking Conference (WCNC'2021)*, 2021, pp. 1–6.
[27] Z. Qin and J. A. McCann, "Resource efficiency in low-power wide-area networks for IoT applications," in *IEEE Global Communications Conference (GLOBECOM'2017)*, December 2017, pp. 1–7.
[28] M. Costa, T. Farrell, and L. Doyle, "On energy efficiency and lifetime in low power wide area network for the Internet of Things," in *IEEE Conference on Standards for Communications and Networking (CSCN'2017)*, September 2017, pp. 258–263.
[29] B. Su, Z. Qin, and Q. Ni, "Energy efficient uplink transmissions in LoRa networks," *IEEE Transactions on Communications*, pp. 1–1, 2020.
[30] T. Elshabrawy and J. Robert, "Analysis of BER and Coverage Performance of LoRa Modulation under Same Spreading Factor Interference," in *2018 IEEE 29th Annual International Symposium on Personal, Indoor and Mobile Radio Communications (PIMRC)*, 2018, pp. 1–6.
[31] O. Afisiadis, M. Cotting, A. Burg, and A. Balatsoukas-Stimming, "On the error rate of the LoRa modulation with interference," *IEEE Transactions on Wireless Communications*, vol. 19, no. 2, pp. 1292–1304, 2020.
[32] F. Orfei, C. B. Mezzetti, and F. Cottone, "Vibrations powered LoRa sensor: An electromechanical energy harvester working on a real bridge," in *2016 IEEE SENSORS*, October 2016, pp. 1–3.
[33] W. Lee, M. J. W. Schubert, B. Ooi, and S. J. Ho, "Multi-source energy harvesting and storage for floating wireless sensor network nodes with long range communication capability," *IEEE Transactions on Industry Applications*, vol. 54, no. 3, pp. 2606–2615, May 2018.
[34] M. Magno, F. A. Aoudia, M. Gautier, O. Berder, and L. Benini, "WULoRa: An energy efficient IoT end-node for energy harvesting and heterogeneous communication," in *Design, Automation Test in Europe Conference Exhibition (DATE'2017)*, March 2017, pp. 1528–1533.
[35] X. Ouyang, O. A. Dobre, Y. L. Guan, and J. Zhao, "Chirp spread spectrum toward the Nyquist signaling rate—orthogonality condition and applications," *IEEE Signal Processing Letters*, vol. 24, no. 10, pp. 1488–1492, 2017.
[36] B. Reynders and S. Pollin, "Chirp spread spectrum as a modulation technique for long range communication," in *2016 Symposium on Communications and Vehicular Technologies (SCVT)*, 2016, pp. 1–5.
[37] M. Chiani and A. Elzanaty, "On the LoRa modulation for IoT: Waveform properties and spectral analysis," *IEEE Internet of Things Journal*, vol. 6, no. 5, pp. 8463–8470, 2019.
[38] A. Mahmood, E. Sisinni, L. Guntupalli, R. Rondón, S. A. Hassan, and M. Gidlund, "Scalability analysis of a LoRa network under imperfect orthogonality," *IEEE Transactions on Industrial Informatics*, vol. 15, no. 3, pp. 1425–1436, March 2019.
[39] L. Amichi, M. Kaneko, E. H. Fukuda, N. El Rachkidy, and A. Guitton, "Joint allocation strategies of power and spreading factors with imperfect orthogonality in LoRa networks," *IEEE Transactions on Communications*, vol. 68, no. 6, pp. 3750–3765, 2020.
[40] C. Caillouet, M. Heusse, and F. Rousseau, "Optimal SF allocation in LoRaWAN considering physical capture and imperfect orthogonality," in *IEEE Global Communications Conference (GLOBECOM'2019)*, Waikoloa, United States, December 2019.
[41] [Online]. Available: https://www.semtech.com/products/wireless-rf/lora-24ghz/sx1281
[42] J. Tapparel, O. Afisiadis, P. Mayoraz, A. Balatsoukas-Stimming, and A. Burg, "An open-source LoRa physical layer prototype on GNU radio," in *2020 IEEE 21st International Workshop on Signal Processing Advances in Wireless Communications (SPAWC)*, 2020, pp. 1–5.
[43] [Online]. Available: https://www.semtech.com/products/wireless-rf/lora-24ghz

Fatma Benkhelifa (SM'12, M'17) is a lecturer in Electrical and Electronic Engineering at Coventry University, UK. She was a research fellow in the AESE research lab at Imperial College London. She obtained her PhD in Electrical Engineering in 2017 from King Abdullah University of Science and Technology (KAUST), Saudi Arabia. She also obtained her Master of Science from KAUST in January 2013. She graduated as a Polytechnician engineer from "Ecole Polytechnique de Tunis" with major in Signals and Systems. Her research interests include, but not limited to, the scalability and coverage of low power wide area networks via resource management algorithms, stochastic geometry-based analysis, and spatiotemporal modelling of wireless sensor networks.

Yathreb Bouazizi (SM'20) joined the AESE research group as a PhD student in 2019. She received her Master of science in ECE (Electrical and Computer engineering) from Georgia Institute of Technology. She also graduated as an engineer in telecommunications from the higher school of communications of Tunis (Sup'Com). She is conducting her research under the Land and Liveability National Innovation Challenge (L2NIC) Research Programme funded by Singapore Ministry of National Development. Her research interests cover the area of low power wide area networks (LPWANs); modelling, performance analysis, and optimisation.

Julie A. McCann (M'16) is a Professor in Computer Systems with Imperial College London. Her research centres on decentralized and self-organizing schemes for spatial computing e.g., Wireless Sensor systems, Internet of Things, or Cyber-physical systems. She leads the Adaptive Embedded Systems Engineering Research (AESE) Lab , is Deputy Director for the UK-wide PeTraS Centre for IoT Cyber-security, and until recently co-directed the Intel Collaborative Research Institute for Sustainable Cities. She has received significant funding though national and international bodies such as the UK's EPSRC, EU FP7/H2020 funding and Singapore NRF; she has a sub-lab in Singapore with I2R and HDB. Prof McCann is an Elected Peer for the EPSRC, serves on/chairs/AE for the top international conference committees and journals in the field, and is a Fellow of the BCS and Chartered Engineer.